



PhD. Thesis

---

# Effects of isospin symmetry breaking in light mesons and application to the anomalous magnetic moment of the muon

---

M.Sc. Jan Bonnet

January 2018

INSTITUTE FOR THEORETICAL PHYSICS  
JUSTUS-LIEBIG-UNIVERSITÄT GIESSEN



Danke an Christian, dass er mich so lange ausgehalten hat.

Danke an Richard, dass er sich mit mir über alles aufregen kann.

Danke an Yannik, dass er mir gesagt hat, dass ich das schaffe.

Und Danke an Jacqueline, dass sie für immer für mich da ist.



# Contents

|          |  |           |
|----------|--|-----------|
| <b>1</b> | <b>Introduction</b>  | <b>1</b>  |
| <b>2</b> | <b>Framework</b>   | <b>5</b>  |
| 2.1      | From Lagrangian to quark . . . . .                             | 5         |
| 2.2      | Rainbow-Ladder and Maris-Tandy model . . . . .                 | 8         |
| 2.3      | Solving the complex quark . . . . .                            | 11        |
| <b>3</b> | <b>Isospin in the meson sector</b>                             | <b>15</b> |
| 3.1      | Mesons in DSE/BSE . . . . .                                    | 15        |
| 3.2      | Modeling QED . . . . .   | 20        |
| 3.3      | Discussion of the results . . . . .                            | 24        |
| <b>4</b> | <b>Application to the anomalous magnetic moment of leptons</b> | <b>35</b> |
| 4.1      | Magnetic moments . . . . .                                     | 35        |
| 4.2      | Standard model contributions to $g - 2$ . . . . .              | 37        |
| 4.3      | Experiment . . . . .   | 42        |
| 4.4      | Hadronic vacuum polarization . . . . .                         | 45        |
| 4.5      | Results in HVP . . . . .                                       | 50        |
| <b>5</b> | <b>Corrections to couplings and the weak mixing angle</b>      | <b>53</b> |
| 5.1      | Electromagnetic coupling . . . . .                             | 53        |
| 5.2      | $SU(2)_L$ coupling and the weak mixing angle . . . . .         | 55        |
| <b>6</b> | <b>Summary</b>   | <b>59</b> |
| <b>7</b> | <b>Appendix</b>  | <b>63</b> |
| 7.1      | Hyperspherical coordinates . . . . .                           | 63        |
| <b>8</b> | <b>Bibliography</b>  | <b>65</b> |



# 1 Introduction

Matter, as we know it from everyday life, consists of bound states that are composed by only a few elementary particles, such as e.g. quarks or electrons. The dynamics between elementary particles resulting in the formation of bound states as well as the stability thereof are governed by fundamental interactions. The theoretical description of these fundamental interactions is summarized in the standard model of particle physics (SM), set up in its present day formulation. The SM describes all interactions of particles as an exchange of a (gauge)boson between the elementary fermionic particles of the respective interaction. It distinguishes between electromagnetic (QED), weak and strong force (QCD), exchanging photons,  $Z$  and  $W$  bosons, and gluons between leptons and quarks. While QED and the weak theory can be treated perturbatively due to weak coupling constants, the gauge boson of the strong theory interacts, as the name states, too strongly to allow for a perturbative approach.

Experimentally, physicists around the world investigate the standard model in all its particulars. Singular aspects, as the measurement of the anomalous magnetic moments of leptons, are subject to intense focused experimental effort. We will elaborate on some of these measurements later in this thesis. At the same time, a host of large experiments such as PANDA or CBM at FAIR center will take a plethora of data with the goal of observing exotic particles, in-medium effects of hadronic matter or even quark-gluon-plasma. Each of these experimental settings strives to contribute more detailed information on different states of matter under more or less extreme conditions in order to better understand, refine or even adjust our formulation of the SM and to fill in the 'white spots' on our experimental maps.

From a theoretical point of view, it is a tremendous task to analyze and describe how the formation of bound states from these basic particles takes place. Already in the nineteen-sixties [1], the predecessor of today's model got introduced and was continuously refined to today's different modern forms. In this thesis, we focus on the most basic bound state matter, the mesons, and their influence on the anomalous magnetic moment of the muon. These states consist of a quark and an antiquark partner. Quarks were introduced by Gell-Mann and Zweig and believed to be a purely mathematical method. Later, they were proved to be real particles by deep inelastic scattering of electrons on nucleons [2, 3]. Gell-Mann and Zweig's quark model allows to draw up particle spectra and multiplets sorted by quark content. In fig. 1.1 we show the multiplets for pseudoscalar and vector mesons [4], parts of both further

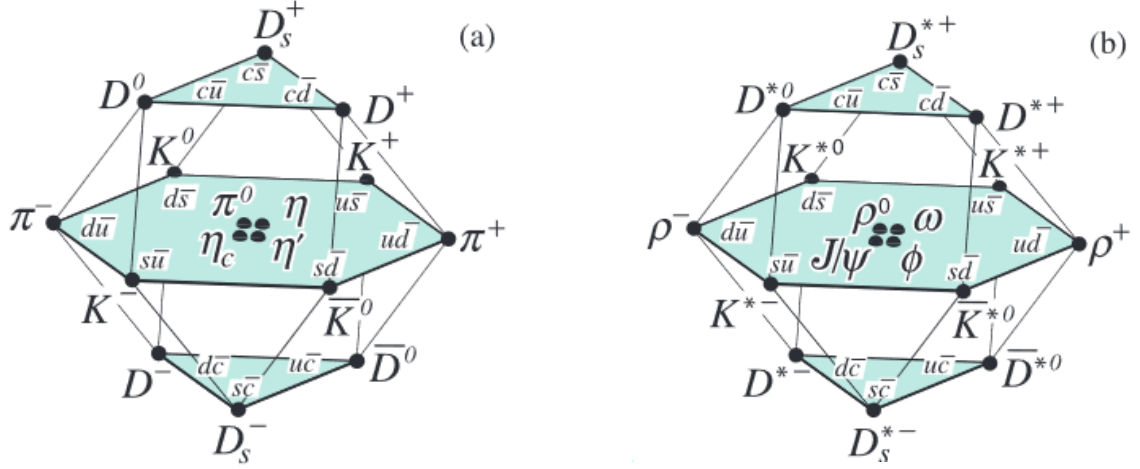


Figure 1.1: Picture (a) shows the multiplet for pseudoscalar and (b) for vector mesons in a quark content representation. The definition of quark content allows to order mesons in a systematic way. Axes denote the third component of isospin (sorting for  $u$  and  $d$  content), charm content and hypercharge, which gives us the strange content. [4]

discussed and investigated later on.

More suited for the description and, in consequence, analysis of the nonperturbative phenomena, are lattice gauge theory or functional methods. These are, for instance, Dyson-Schwinger equations (DSE) [5,6] or functional renormalization group approaches. A common feature of these are quarks and gluons as fundamental degrees of freedom. Each of these methods has its own strengths and weaknesses. While lattice gauge theory is often considered as 'theoretical measurement', it is limited by the involved numerics, in particular the often unphysical quark or pion masses, finite volume effects or other technical problems. Most settings also need to connect separate fits for high energy and low energy regions with a Heaviside step function. Nevertheless, the lattice, implemented in a correct way, is an invaluable tool to investigate QCD physics.

A complementary approach to lattice calculations are the above mentioned functional methods. This becomes more obvious considering for example their benefits of dynamical chiral symmetry breaking, a continuous treatment of the transition from low to high energy regime and - compared to lattice gauge theory studies- overwhelmingly short computation times. The main disadvantage of functional methods is the need to truncate the 'infinite tower of DSEs', which we will further explain



---

in chapter 2. In the past, descriptions of bound states and their form factors in the framework of Dyson-Schwinger and Bethe-Salpeter equations (BSE) have been very successful [7–24], not only in the field of simple mesons, but also investigating baryons, excited states or even tetra-quarks.

Also, functional methods have a history of successful calculations for the above mentioned anomalous magnetic moments [25–29]. We try to provide a fresh look at some of these. The focus of this work lies in isospin symmetry breaking in processes formerly described without these considerations. For many applications it is sufficient to use approximate isospin symmetry, treating the up ( $u$ ) and down ( $d$ ) quark as an averaged particle  $\bar{u}d$ . In this work, we want to investigate the effect of a modified QCD/QED model for our DSE/BSE framework. This model lifts the current quark mass degeneracy and in a second step includes charge dependency to the calculation of quark propagator, meson mass and amplitudes and the quark-photon vertex. The establishment of the model and tests on the hadronic vacuum polarization (HVP) as a part of the anomalous magnetic moments of muon and tau, are the first results in this framework where the assumptions of isospin symmetry are lifted. As a further application of the model, we followed the calculations of [30] and compare our results to their corrections of  $\alpha_{QED}$  and the weak mixing angle.

The thesis is structured in the following way.

In chapter 2, basic concepts of QCD in general, and functional methods in particular are laid out. We start from the QCD Lagrangian in order to exemplarily construct the DSE for the quark propagator. As a next step, we proceed to explain the Rainbow-Ladder (RL) truncation and the Maris-Tandy (MT) interaction model for  $\alpha_{QCD}$ , that is used in the following thesis. Since we numerically restrict ourselves to specific ways to solve the quark, we also present the employed method at this point. Even though this chapter represents a compilation of techniques one could find in textbooks or publications, we consider this synopsis helpful, in order to understand the basic toolbox before interpreting the results presented in the later chapters.

Next, we focus on isospin symmetry and its implications for the meson sector in chapter 3. We describe how meson masses and amplitudes can be calculated by solving a BSE. Following our general explanations, we explicitly use the solved BSEs for the light meson sector and extend the previously introduced method with QED contributions and mass splitting to investigate isospin symmetry breaking. In this context, we also probe the influence of the described changes to the vector meson channel. Summarizing the chapter, we discuss our new QCD/QED model and the resulting meson masses.

In chapter 4, we give an overview over leptonic magnetic moments and the hadronic vacuum polarization in the DSE/BSE framework. We present how we are finally able to apply our model to the HVP problem. The final part of the chapter discusses the latest DSE/BSE results for muon and tau. These are, together with the model parameters themselves, the main results of this thesis.

As mentioned earlier, the possibility to utilize our method to calculate corrections to the electromagnetic coupling and the weak mixing angle was brought to our attention. The explicit implementation as well as results are compiled in chapter 5.

We close with an overall summary of the findings and challenges of our investigations in Chapter 6 and provide an outlook on interesting aspects of the topic that might be subject of future research.

## 2 Framework

This chapter summarizes the necessary steps to start at the Lagrangian and end up with a strategy to solve the Dyson-Schwinger equation of the quark. On the way, we cover some 'must knows' such as the way to arrive at the equation we want so solve, the truncation and the modeling needed. The chapter concludes with an explanation why and how we solve the quark in a specific way.

### 2.1 From Lagrangian to quark

The euclidean gauge fixed Lagrangian of QCD  $\mathcal{L}_{QCD}$  and thus the starting point of our investigation reads as

$$\begin{aligned}\mathcal{L}_{QCD} = & Z_2 \bar{\psi} (-\not{\partial} + Z_m m) \psi + Z_3 \frac{1}{2} A_\mu^a \left( -\partial^2 \delta_{\mu\nu} - \left( \frac{1}{Z_3 \xi} - 1 \right) \partial_\mu \partial_\nu \right) A_\nu^a \\ & + \tilde{Z}_3 \bar{c}^a \partial^2 c^a - Z_{1F} i g \bar{\psi} \gamma_\mu t^a \psi A_\mu^a - Z_1 g f^{abc} (\partial_\mu A_\nu^a) A_\mu^b A_\nu^c \\ & + Z_4 \frac{1}{4} g^2 f^{abe} f^{cde} A_\mu^a A_\nu^b A_\mu^c A_\nu^d + \tilde{Z}_1 g f^{abc} \bar{c}^a \partial_\mu (A_\mu^c c^b) .\end{aligned}\quad (2.1)$$

This construct is built by particle fields of the theory;  $\psi$  for quarks,  $A_\mu^a$  for gluons and  $c$  for the unphysical Faddeev-Popov ghosts that were introduced to enforce gauge fixing.  $t$  denotes the generator of color  $su(3)$ , and  $f^{abc}$  the total antisymmetric structure constant.  $\xi$  is the gauge parameter and  $g$  the strong coupling constant. The current quark mass is labeled  $m$ . QCD is a multiplicative renormalizable theory, which means that divergences in fields and vertices can be countered by the introduction of renormalization constants  $Z_*$ . Expressing all these constants in terms of renormalizations of fields and the coupling, we get the relations

$$Z_{1F} = Z_g Z_2 Z_3^{1/2}, \quad Z_1 = Z_g Z_3^{3/2}, \quad \tilde{Z}_1 = Z_g \tilde{Z}_3 Z_3^{1/2}, \quad Z_4 = Z_g^2 Z_3^2. \quad (2.2)$$

As a result of the Becchi-Rouet-Stora-Tyutin symmetry (BRST) [31], Slavnov-Taylor identities (STI) [32, 33] and by working in Landau gauge  $\xi = 0$ , we can also use

$$\frac{Z_4}{Z_1} = \frac{Z_1}{Z_3} = \frac{\tilde{Z}_1}{\tilde{Z}_3} = \frac{Z_{1F}}{Z_2} \quad (2.3)$$

and

$$\tilde{Z}_1 = 1. \quad (2.4)$$

From the Lagrangian, we define the generating functional  $Z$ , using the classical action  $S[\Phi] = \int d^4x \mathcal{L}[\Phi]$ .  $\Phi$  is a superfield enclosing all fields in the theory and  $J$  the correlated supersource.

$$Z[J] = \int \mathcal{D}\Phi e^{-S[\Phi] + \int d^4x J_a(x) \Phi_a(x)} \quad (2.5)$$

The path integral  $\int \mathcal{D}\Phi$  covers all fields at all space-times. We apply the assumption that the generating functional falls off quickly enough at large space-time points. Thus any surface terms vanish, we can write

$$0 = \int \mathcal{D}\Phi \frac{\delta}{\delta \Phi} e^{-S[\Phi] + J_i \Phi_i} = \int \mathcal{D}\Phi e^{-S[\Phi] + J_i \Phi_i} \left( \frac{\delta S[\Phi]}{\delta \Phi_i} - J_i \right) \quad (2.6)$$

which is the vacuum expectation value of the bracket enclosed term in the presence of a source.

$$0 = \left\langle \frac{\delta S[\Phi]}{\delta \Phi_i} - J_i \right\rangle_{[J]}. \quad (2.7)$$

Expressing the field  $\Phi$  with the derivative of its source  $\Phi_i \rightarrow \frac{\delta}{\delta J_i}$  acting on the generating functional, we arrive at the master DSE. All other equations for the full 1PI Greens functions can be derived from this seed equation. A more detailed description can be found in [34, 35]

$$\left( \frac{\delta S}{\delta \Phi_i} \Big|_{\Phi_i \rightarrow \frac{\delta}{\delta J_i}} - J_i \right) Z[J] = 0 \quad (2.8)$$

To solve for a specific equation, one has to apply the functional derivatives corresponding to the sources of interest and set said sources to zero afterwards. For our concerns, the most used equation is the Dyson-Schwinger equation for the quark propagator. Employing the explicit derivative  $\delta/\delta \bar{\psi}(x)$  and source  $j(x)$  for an anti-quark at given space-time point  $x$ , we get

$$\left\langle \frac{\delta S_{QCD}}{\delta \bar{\psi}(x)} - j(x) \right\rangle_{[J]} = 0. \quad (2.9)$$

Performing another derivative with respect to the source  $j$  at a second space-time point  $y$ , we arrive at

$$\left\langle \frac{\delta S_{QCD}}{\delta \bar{\psi}(x)} \bar{\psi}(y) \right\rangle_{[J]} - \delta^4(x - y) = 0. \quad (2.10)$$

Now we are able to insert the QCD Lagrangian, perform the derivative and set all leftover sources to zero. The resulting equation

$$\begin{aligned} \delta^4(x - y) &= Z_2 (-\not{\partial} + Z_m m) S(x - y) \\ &\quad - ig Z_{1F} \int d^4z d^4z' \delta^4(x - z) \delta^4(x - z') \gamma^\mu \frac{\lambda^a}{2} \langle \psi(z) \bar{\psi}(y) A_\mu^a(z') \rangle \end{aligned} \quad (2.11)$$

is the quark DSE in coordinate space, where  $S(x - y)$  is the fully dressed quark propagator

$$S(x - y) = \langle 0 | \psi(x) \bar{\psi}(y) | 0 \rangle \quad (2.12)$$

while  $\langle \psi(z) \bar{\psi}(y) A_\mu^a(z') \rangle$  can be identified as the quark-quark-gluon vertex  $-igt^a \Gamma_\mu$ . Since all calculations in this thesis were performed in euclidean momentum space, we end the derivation with equation 2.13

$$S^{-1}(p) = Z_2(i\not{p} + Z_m m) + g^2 Z_{1F} C_f \int \frac{d^4 k}{(2\pi)^4} \gamma^\mu S(k) \Gamma^\mu(k, q) D_{\mu\nu}(q), \quad (2.13)$$

where  $D_{\mu\nu}(q)$  denotes a gluon propagator and  $q = p - k$ . The Casimir  $C_f = t^a t^a$  can be immediately evaluated to

$$C_f = (N_c^2 - 1)/2N_c = 4/3. \quad (2.14)$$

The presence of the quark-gluon vertex shows an underlying challenge of the functional Dyson-Schwinger method, which will be tackled in the next section.

## 2.2 Rainbow-Ladder and Maris-Tandy model

Any given equation we generate in this manner will inevitably include a higher lying Greens function. To calculate this function, one would need to solve the corresponding DSE and subsequently end up at the next higher order. This phenomenon is called the infinite tower of DSEs. Obviously, it is impossible to solve a system of infinitely many coupled equations. To get any quantitative results, a truncation of the system is needed. Note that up to this point no simplifications were made, the equation itself is exact.

The most common method used in our field of research is the so called Rainbow-Ladder truncation, where the quark-vertex and the gluon propagator are treated as closed expressions and thus the quark DSE can be solved directly. Mathematically, we reduce the Dirac structure of the full quark-gluon vertex to its leading component. The full vertex would have the form

$$\Gamma_\mu(p, q) = \sum_i^{12} T_\mu^i(p, q) \lambda^i(p, q), \quad (2.15)$$

with  $T^i$  denoting tensor structures and  $\lambda^i$  their dressing functions. Here,  $p$  denotes the quark and  $q$  the gluon momentum. The basis for the vertex would be linear combinations of

$$\{\gamma_\mu, p_\mu, q_\mu\} \otimes \{\mathbb{1}, \not{p}, \not{q}, [\not{p}, \not{q}]\}. \quad (2.16)$$

Rainbow-Ladder now reduces the number of tensor structures to one, with the scalar dressing function  $\Gamma^{\text{RL}}$  as a function of only the squared gluon momentum.

$$\Gamma_\mu(p, q) \simeq \gamma_\mu \Gamma^{\text{RL}}(q^2). \quad (2.17)$$

Next, we take a closer look at the gluon propagator

$$D_{\mu\nu}(q) = \left( \delta_{\mu\nu} - \frac{q_\mu q_\nu}{q^2} \right) \frac{Z(q^2)}{q^2} = T_{\mu\nu}(q) \frac{Z(q^2)}{q^2}, \quad (2.18)$$

where the only unknown is the scalar dressing  $Z(q^2)$ . Combining both dressings for gluon and vertex to an effective interaction  $\alpha_{\text{eff}}(q^2)$  leads to

$$Z_{1F} \frac{g^2}{4\pi} Z(q^2) \Gamma^{\text{RL}}(q^2) = Z_2^2 \alpha_{\text{eff}}(q^2). \quad (2.19)$$

The renormalization behavior stems from the fact that we can use the STI for  $Z_{1F} = Z_g Z_2 Z_3^{1/2}$  and know that  $g$  scales as  $1/Z_g$ , the vertex as  $Z_{1F}$  and the gluon propagator as  $1/Z_3$ .

Furthermore we use the axial-vector Ward-Takahashi identity (AxVWTI) [7, 36–38], which relates the quark-antiquark interaction via the axial-vector vertex to the quark propagator:

$$iP_\mu \Gamma_{5\mu}^f(p, P) = S^{-1}(p - P/2) \gamma_5 t^f + \gamma_5 t^f S^{-1}(p + P/2). \quad (2.20)$$

Here  $P$  and  $p$  are the total and relative momenta of the quarks, and  $t^f$  generators of the axial  $U_A(N_f)$  flavor symmetry. In the case of RL truncation, the extracted quark-antiquark interaction kernel reads

$$iK^{q\bar{q}} = 4\pi Z_2^2 \frac{\alpha_{eff}(q^2)}{q^2} T_{\mu\nu}(q) (i\gamma^\mu) \otimes (i\gamma^\nu). \quad (2.21)$$

The interaction can be seen as a single dressed gluon exchange between the quark and its anti-partner. This treatment ensures the Goldstone boson behavior of pseudoscalar mesons in the absence of a current mass.

An effective interaction needs to satisfy certain requirements. First of all it should preserve symmetries if possible. Secondly, it is desirable to approach logarithmic running of the coupling for high momenta, reproducing perturbative behavior. Thirdly, a certain strength in the IR region will produce dynamical chiral symmetry breaking. A very successful model which incorporates all these properties is the Maris-Tandy model [10]. It reads

$$\alpha_{eff}(q^2) = \frac{\pi}{\omega^6} D q^4 \exp\left(-\frac{q^2}{\omega^2}\right) + \frac{2\pi\gamma_m[1 - \exp(-q^2/(4m_t^2))]}{\log(\tau(1 + q^2/\Lambda_{QCD}^2))}, \quad (2.22)$$

with  $\omega = 0.4$  GeV and  $D = 0.93$  GeV<sup>2</sup>. The other parameters are  $\gamma_m = 12/(33 - 2N_f)$  the anomalous dimension of the quark propagator,  $m_t = 0.5$  GeV,  $\tau = e^2 - 1$  and  $\Lambda_{QCD} = 0.234$  GeV.  $N_f$ , the number of quark flavors is usually set to 4. Another representation of the MT-parameters is  $\eta$  and  $\Lambda$  instead of  $\omega$  and  $D$ . These notations are related by

$$\omega = \frac{\Lambda}{\eta} \quad \text{and} \quad D = \eta\Lambda^2. \quad (2.23)$$

Above mentioned standard values translate to  $\eta = 1.8$  and  $\Lambda = 0.72$  GeV [39]. For completeness it should be mentioned that we modify the effective interaction with a Pauli-Villars regulator

$$\alpha_{eff}(q^2) \rightarrow \alpha_{eff}(q^2) \frac{1}{1 + q^2/PV^2} \quad (2.24)$$

of size  $PV = 200$  GeV for the numerical calculations, which in turn modifies  $\Lambda = 0.74$  GeV to keep the pion decay constant intact.

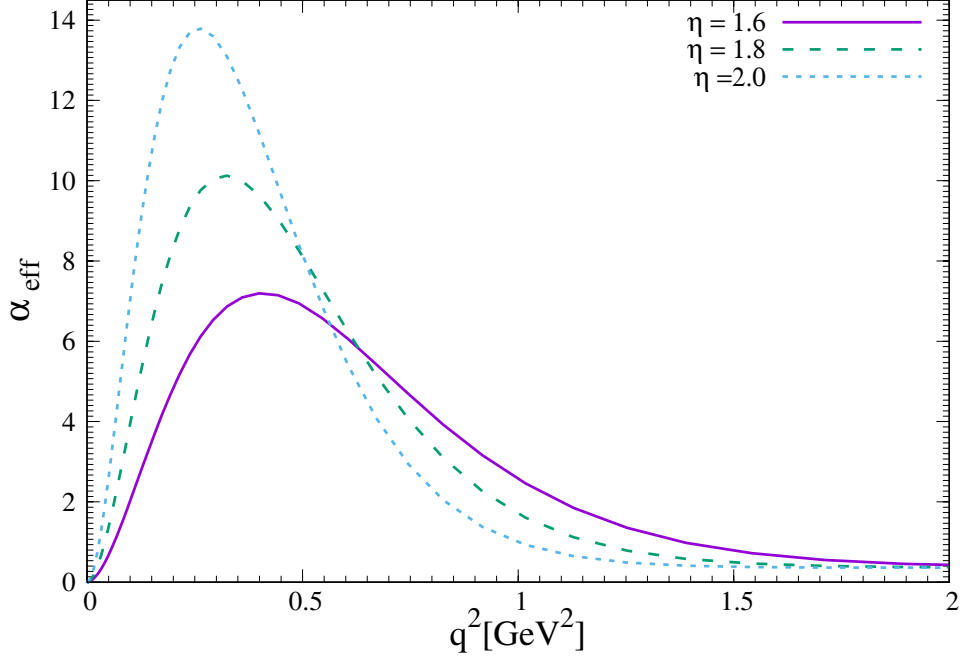


Figure 2.1: A different model parameter  $\eta$  defines the shape of the MT effective interaction. The perturbative running for high momenta is not changed, while the IR behavior regulates chiral symmetry breaking. We show  $\alpha_{eff}$  for  $\eta = 1.6$ ,  $\eta = 1.8$  and  $\eta = 2.0$ . For our calculations, we use  $\eta = 1.8$ .

As we wished for,  $\alpha_{eff}$  approaches the one-loop coupling of QCD for  $q^2 \gg \Lambda_{QCD}^2$ . In the standard setting, the parameters  $\omega$  and  $D$  are used to fit the model to the physical pion decay constant  $f_\pi$ .

The research on beyond Rainbow-Ladder [11, 40–42] is a highly challenging field, but in the scope of this thesis, we restrict ourselves to the Rainbow-Ladder truncation with MT-model.



## 2.3 Solving the complex quark

Now that we decided on a truncation and an effective coupling, we take a look at equation 2.13 again. After we are done inserting equations 2.17, 2.18 and 2.19, the system we have to solve is

$$S^{-1}(p) = Z_2(i\not{p} + Z_m m) + 4\pi Z_2^2 C_f \int \frac{d^4 k}{(2\pi)^4} T_{\mu\nu}(q) \gamma^\mu S(k) \gamma^\nu \frac{\alpha_{eff}(q^2)}{q^2}. \quad (2.25)$$

The general structure of  $S^{-1}(p)$  and  $S(p)$  are

$$S^{-1}(p) = i\not{p}A(p^2) + B(p^2) \quad \text{and} \quad S(p) = \frac{-i\not{p}A(p^2) + B(p^2)}{p^2 A^2(p^2) + B^2(p^2)}, \quad (2.26)$$

where  $A$  and  $B$  are scalar dressing functions. These dressings are related to the quark wave function renormalization  $Z_\psi$  and the quark mass function  $M$  by

$$Z_\psi(p^2) = \frac{1}{A(p^2)} \quad \text{and} \quad M(p^2) = \frac{B(p^2)}{A(p^2)}. \quad (2.27)$$

To solve for these dressing functions, simple projections are applied to equation 2.25. For the extraction of  $B$ , tracing the equation is enough. For  $A$ , a possible projection is to multiply by  $\not{p}$  and trace afterwards. The resulting system of two coupled integral equations can be solved numerically straight forward. We use naive fixed point interaction and hyperspherical coordinates for the integrals, see appendix 7.1. At the moment, any result would still depend on the chosen cutoff of the integral. To find meaningful results we need to apply a scheme to relate calculations to a fixed renormalization point  $\mu$ . We demand of our system the properties

$$A(\mu^2) = 1 \quad B(\mu^2) = m_q \quad (2.28)$$

where  $m_q$  is the quark flavor dependent current mass. A standard value for the renormalization point is  $\mu = 19$  GeV. We traded the cutoff dependency for a  $\mu$  dependency, which is a much better point of reference when there is need to compare different calculations. Figure 2.2 shows the quark DSE in diagram form.

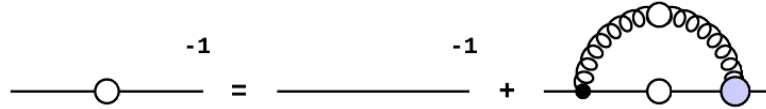


Figure 2.2: The dressed quark propagator (left side) is the heart of our calculations. It contains the bare propagator and the hadronic quark self energy. The self energy diagram contains the dressed quark itself, the dressed gluon and the dressed quark-gluon vertex. Depending on notation, the two diagrams are connected by a '+' or a '-' sign.

Thus we solved the quark propagator for a given real momentum  $p$ . Usual current masses used for calculations are listed in table I. These quark masses were determined to produce the correct masses pseudoscalar and vector mesons. For the averaged  $\bar{u}d$  and the  $s$  quark pion and kaon were used [10], for  $c$  the vector  $J/\Psi$  [12], and for  $b$  the bottomonium ground states, especially the  $Y(1S)$  [22].

| $m_{\bar{u}d}$ | $m_s$ | $m_c$ | $m_b$ |
|----------------|-------|-------|-------|
| 3.7            | 85    | 827   | 3680  |

Table I: Standard current masses for quarks used in DSE/BSE calculations. The masses, together with the MT parameters are chosen to reproduce light meson properties as bound state masses and decay constants,  $J/\Psi$ , and bottomonium ground states. All masses are given in MeV.

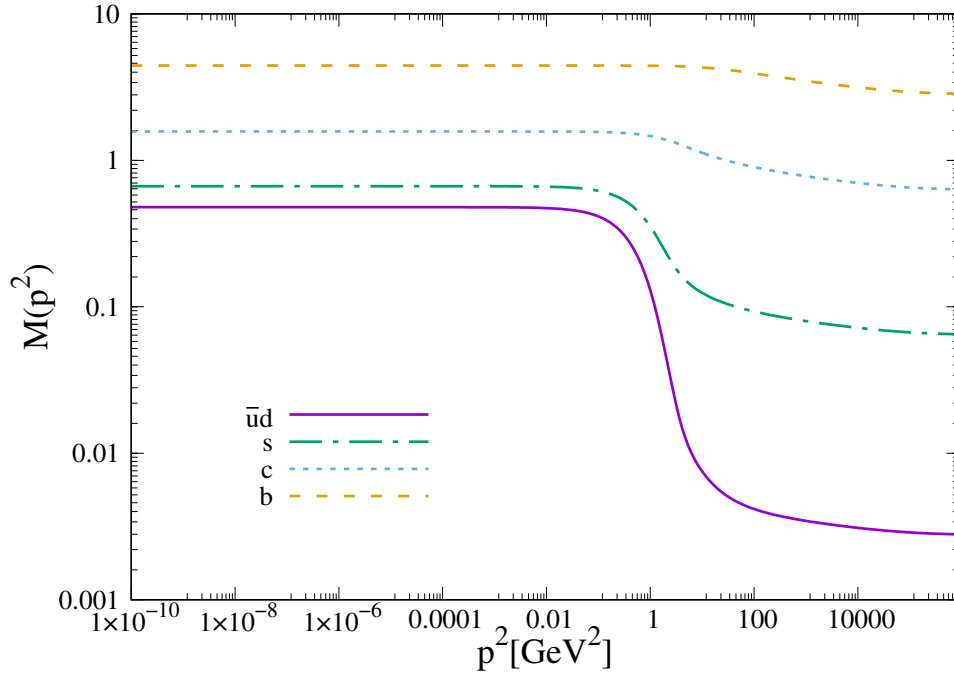


Figure 2.3: A standard set of quark masses as shown in table I used with the RL-MT truncation produces quark mass functions as shown here. We see the the chiral symmetry breaking in the mass function. At the renormalization point  $\mu$ , the mass function is fixed to the quark current masses.

When it comes to bound states, such as mesons we will need to extend the procedure to the complex plane. A straight forward way to do this is to route the complex part of the momentum through the gluon. This allows us to insert our real quark in the equation for the complex quark. Then, we perform the integral only once instead of doing a complex iteration. This is possible since we have an expression for the effective interaction, which does not explicitly depend on the quark dressing functions. Unfortunately, we will not be able to use this method for all calculations in this thesis. We have to find other means to get complex expressions for  $A$  and  $B$ .

One such way [43, 44] is the use of Cauchy's Theorem, which implies that a function  $f$  at a given point  $p^2$  can be found by integrating over a closed contour  $C$  via

$$f(p^2) = \frac{1}{2i\pi} \oint_C dq^2 \frac{f(q^2)}{q^2 - p^2} \quad (2.29)$$

To find a proper contour, we look into the momentum region we are actually interested in. First we change the momentum routing from passing the external (and thus now complex) momentum  $p$  through the gluon via  $q = p - k$ , to passing it through the internal quark. The loop momentum is now  $q^2$ , while the momentum evaluated in the internal quark reads as

$$k^2 = p^2 + q^2 + 2(p \cdot q) \quad (2.30)$$

These probed points are, for a fixed momentum  $p$ , located on the shape of a parabola. This parabola in turn is enclosed by a parabola parameterized as

$$p^2 = x - \frac{1}{4}M^2 \pm iM\sqrt{x} \quad (2.31)$$

for any given  $p^2$  with  $x \in \{0, \Lambda^2 + M^2/4\}$ , as long as the real part of the squared momentum  $k^2$  is lower than the upper bound of  $x$ .  $M$  and  $\Lambda$  define the shape of the parabola where  $M$  fixes the apex and  $\Lambda$  relates this representation to the cutoff formerly used in the self energy integral. Together they define the new cutoff  $\tilde{\Lambda}$ , at which both ends of the parabola are connected with a straight line to finalize the closed contour we need. In reality, also values slightly higher than  $\tilde{\Lambda}^2$  are tested, but the change compared to values lying on the contour is numerically negligible, so it is sufficient to use these instead of performing involved extrapolations.

In terms of quadrature rules, we can express equation 2.29 in a numerically approachable form:

$$f(p^2) = \frac{\sum_j \frac{w_j f(q_j^2)}{q_j^2 - p^2}}{\sum_j \frac{w_j}{q_j^2 - p^2}}, \quad (2.32)$$

with

$$2\pi i = \sum_j \frac{w_j}{q_j^2 - p^2} \quad (2.33)$$

Since numerical errors occur for tested inputs close to the contour border, a technical trick is employed [45]. Writing the factor  $2i\pi$  as an interpolation of a function using the same quadrature, basically any error mentioned above is divided out of the system. There are even more sophisticated approaches to the problem of the complex quark which can be found in e.g. [46].

We are now in a position to start investigating bound state physics using the quark propagator in the complex plane and the Rainbow-Ladder/Maris-Tandy Kernel 2.21. The method to do so will be described in the following chapter.

## 3 Isospin in the meson sector

In this chapter we specify the general treatment of mesons in the Dyson-Schwinger/Bethe-Salpeter approach. This allows us to investigate the manifestations of isospin symmetry. We separate and analyze the impact of quark current masses and charge on mesons masses to find a phenomenologically motivated model extension to the functional DSE/BSE approach incorporating isospin symmetry breaking.

### 3.1 Mesons in DSE/BSE

In chapter 1, mesons were introduced as the easiest color neutral combination of quarks and antiquarks, namely one of each with opposite color charge. In the functional DSE/BSE formalism, all related information are encoded in the connected quark-antiquark four point function  $T$ . This object contains any exchange in a given theory between a propagating quark and its antiquark partner. Schematically, we derive the homogeneous BSE for a mesonic bound state by starting with the scattering equation of the  $T$ -Matrix

$$T = K + TSSK, \quad (3.1)$$

as seen in figure 3.1.  $K$  denotes the interaction Kernel, in our case the RL-Kernel from equation 2.21. The quark and antiquark are represented by their propagators  $S$ . For readability, we suppress indice and momentum dependencies. The derivation as it is shown here is of course extremely simplified and only used to get a general idea of the underlying process. For more involved discussion we suggest reading [47, 48].

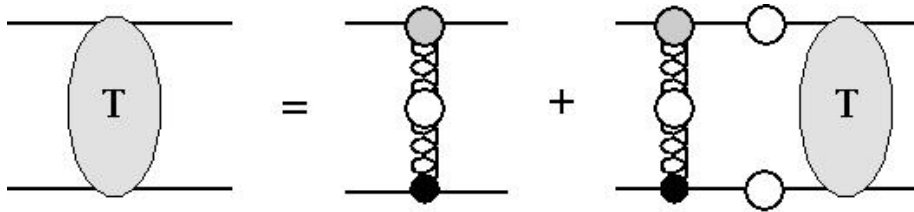


Figure 3.1: The inhomogeneous BSE for the  $T$ -matrix. The right hand side of the equation consists of a 'bare' interaction Kernel in our case the one gluon exchange, and a  $T$ -matrix connected to a Kernel via dressed quarks.

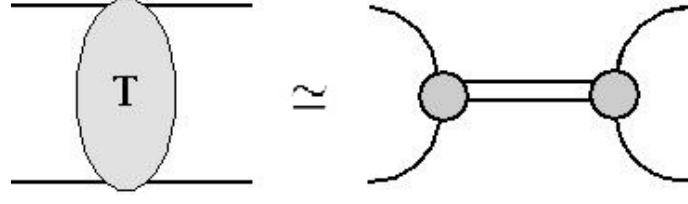


Figure 3.2: Pole representation of  $T$ . The scattering matrix  $T$  can be approximated by a sum of meson poles and regular parts, which are not interesting for our concerns. The meson poles are defined by their bound state amplitudes, which encode the quark-antiquark to meson transformation

Expressing  $T$  in the pole representation (figure 3.2), we get

$$T \simeq \frac{\Gamma \bar{\Gamma}}{P^2 + M^2} + reg \quad (3.2)$$

where  $\Gamma$  is the bound state amplitude of a meson of mass  $M$  and  $reg$  sums up regular and thus irrelevant parts of  $T$ . Plugging in equation 3.2 in equation 3.1 lets us solve for

$$\Gamma = K S S \Gamma, \quad (3.3)$$

which is the homogeneous BSE for mesonic bound states.

Important information we find in this exercise are the fact that any momentum  $P^2$  that solves equation 3.3 corresponds to a bound state.  $P = p_+ - p_-$  is the total momentum of quark ( $p_+ = p + P/2$ ) and antiquark ( $p_- = p - P/2$ ). Any non bound states included in  $T$ , namely scattering states got projected out in the derivation. Solutions for complex squared momenta correspond to resonances, which will not be of further importance in this thesis. Solving the equation itself gives us two connected information, masses and amplitudes. Finding a solution is the theoretical analogue to measuring/detecting mesons in an experiment. The strategy to find these values

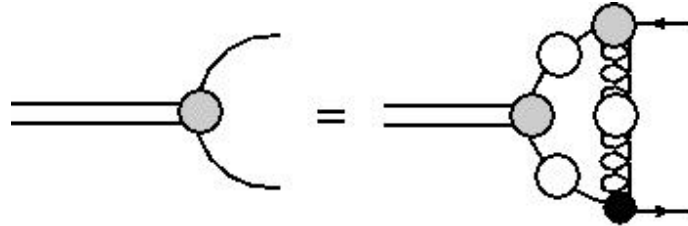


Figure 3.3: The combination of  $T$  matrix BSE and pole representation leads us to the meson bound state BSE. It is valid for bound state momenta  $P^2 = -M^2$ , and solved as an linear algebra eigenvalue problem. Normalization is arbitrary if interest is only in the mass. For the amplitudes an additional condition must be employed.

involves an auxiliary parameter  $\lambda$ . We state

$$\Gamma(P^2) = \lambda(P^2) K S S \Gamma, \quad (3.4)$$

which modifies the equation to resemble an eigenvalue problem, where  $\Gamma$  is the eigenvector. Any value  $P_*^2$  leading to  $\lambda(P_*^2) = 1$  corresponds to a solution of the actual equation 3.3 and thus to a meson mass. Solving an eigenvalue problem for well behaved problems is straight forward.

We can also extract the meson amplitudes related to a bound state of specific mass  $M^2 = -P^2$ . To actually use them, we need to normalize  $\Gamma$ . The normalization condition makes use of the eigenvalue  $\lambda$  again and is defined by [48]

$$\left( \frac{d \ln(\lambda(P^2))}{dP^2} \right)^{-1} \Big|_{P^2=-M^2} \stackrel{!}{=} \bar{\Gamma} S S \Gamma. \quad (3.5)$$

An example where amplitudes are needed would be calculations involving formfactors. For any analyses presented in this thesis they are not directly employed, so normalization is arbitrary.

Translating to a proper mathematical form, we get

$$\Gamma(p, P) = -\frac{4}{3} Z_2^2 \int \frac{d^4 k}{(2\pi)^4} T_{\mu\nu}(q) \gamma_\mu S(k_+) \Gamma(k, P) S(k_-) \gamma_\nu \frac{\alpha_{eff}(q^2)}{q^2} \quad (3.6)$$

where the gluon  $D_{\mu\nu}(q = p - k)$  was treated as in equation 2.18 and  $\alpha_{eff}$  from equation 2.19. The loop momentum  $k$  is, as in the quark, usually integrated over via hyperspherical coordinates.

This equation is a general expression for any meson. To further specify the actual particle of interest, two informations need to be passed. First, we need to define the quark content. This happens strictly in the current mass of the quark propagator, since the effective interactions is flavor blind. Furthermore the quantum numbers of the meson need to be set. This determines how the tensor structure of  $\Gamma$  is defined. We work with pseudoscalar ( $P_{S_i}$ ) and vector ( $V_i$ ) mesons, so we give explicit bases for these states:

$$\begin{aligned} P_{S_1} &= \gamma^5 \\ P_{S_2} &= -\gamma^5 \not{p} \\ P_{S_3} &= -\gamma^5 \not{p} \\ P_{S_4} &= \gamma^5 [\not{p}, \not{p}] \end{aligned} \quad (3.7)$$

$$\begin{aligned}
V_1^\mu &= i\gamma_T^\mu \\
V_2^\mu &= \gamma_T^\mu \not{P} \\
V_3^\mu &= -\gamma_T^\mu \not{p} + p_T^\mu \mathbf{1} \\
V_4^\mu &= i\gamma_T^\mu [\not{P}, \not{p}] + 2ip_T^\mu \not{P} \\
V_5^\mu &= p_T^\mu \mathbf{1} \\
V_6^\mu &= p_T^\mu \not{P} \\
V_7^\mu &= -ip_T^\mu \not{p} \\
V_8^\mu &= p_T^\mu [\not{P}, \not{p}]
\end{aligned} \tag{3.8}$$

The index  $T$  means that the vector/matrix was constructed transversally to  $P$ . These are specific bases, for example listed in [11]. In general, any basis system spanning  $\{\gamma^5, \gamma^5 \not{P}, \gamma^5 \not{p}, \gamma^5 [\not{p}, \not{P}]\}$  can be used for pseudoscalars. Higher spin states can be constructed as described in e.g. [39, 49].

$$\begin{aligned}
\Gamma_{PS}(p, P) &= \sum_{i=1}^4 P_{Si}(p, P) \Gamma_{PS,i}(p, P) \\
\Gamma_V^\mu(p, P) &= \sum_{i=1}^8 V_i(p, P) \Gamma_{V,i}^\mu(p, P)
\end{aligned} \tag{3.9}$$

Now we discretize the integral, and the amplitude elements  $\Gamma_i$  are projected out. Respective projectors can be found using linear algebra methods and need to satisfy

$$\Gamma_i(p, P) = \text{Tr}[P_i^{(\mu)}(p, P) \Gamma^{(\mu)}(p, P)]. \tag{3.10}$$

Applying the projection to equation 3.6 gives an equation system that can be treated as an eigenvalue problem as explained around equation 3.4. We are now able to solve the bound state BSE for pseudoscalar and vector mesons and start focusing at physics.



As mentioned in chapter 1, the  $u$  and  $d$  quark are usually treated as an averaged particle  $ud$ . Using the standard values for quark masses from chapter 2, a collection of meson masses relevant for this thesis and calculated with our numerics is listed in table I. The mass values are averaged for charged and neutral mesons. Pseu-

|     | $M_{\pi^0}$ | $M_{\pi^\pm}$ | $M_{K^0}$ | $M_{K^\pm}$ | $M_{\rho^0}$ | $M_{\rho^\pm}$ | $M_\phi$ |
|-----|-------------|---------------|-----------|-------------|--------------|----------------|----------|
| DSE | 138.2       |               | 495.6     |             | 745.3        |                | 1075.4   |
| Exp | 135         | 139.5         | 497.6     | 493.6       | 775          | 775            | 1020     |

Table I: Standard meson masses in RL-MT with the presented parameter set. Since isospin symmetry does not distinguish between charged and neutral pions, kaons and rhos, the effective interaction is set to produce averaged masses. The experimental values taken from the PDG [4]. All masses are given in MeV.

doscalar mesons, together with their respective decay constant were used to fix the model [10]. To find a proper  $c$  and  $b$  mass, the vector mesons masses  $M_{J/\Psi} = 3.1$  GeV and  $M_{Y(1S)} = 9.46$  GeV were used. Since we did only use the masses and did not calculate the bound states ourself they are not listed in table I. The rho meson is a bit too light while the phi is too heavy. In some cases alternative current quark masses were used in calculations to cover the related vector current physics more precisely [50]. This treatment trades better precision in the vector channel for distorted pseudoscalar masses.

Smaller differences to other publications originate from different specifics as e.g. Pauli-Villars regulators or MT-parameter.

We summarize some limitations of the used methods. All bound states are treated as 'pure' quark states of one defined quark and one defined antiquark. For pion, kaon and rho masses, charged and neutral states are degenerated. In isospin limit,  $u$  and  $d$  quark have the same mass and charge is not included yet. Also, bound states do not have a width using our method.

Before we start modifying our calculations, we remind the reader of an important feature of DSE/BSE systems. The Gell-Mass - Oakes - Renner relation (GMOR) [51] is preserved, even in the 'simple' system of RL-MT. This relation links the quark current mass to the squared pion mass and is a direct implication of the pseudo-goldstone boson nature of the pions. Figure 3.4 shows the calculated values for  $M_\pi^2$  versus the quark mass. We see an almost perfect linear behavior as expected from the relations. In any GMOR like plot we show, the values for the physical masses of neutral and charged pions are marked with a horizontal line.

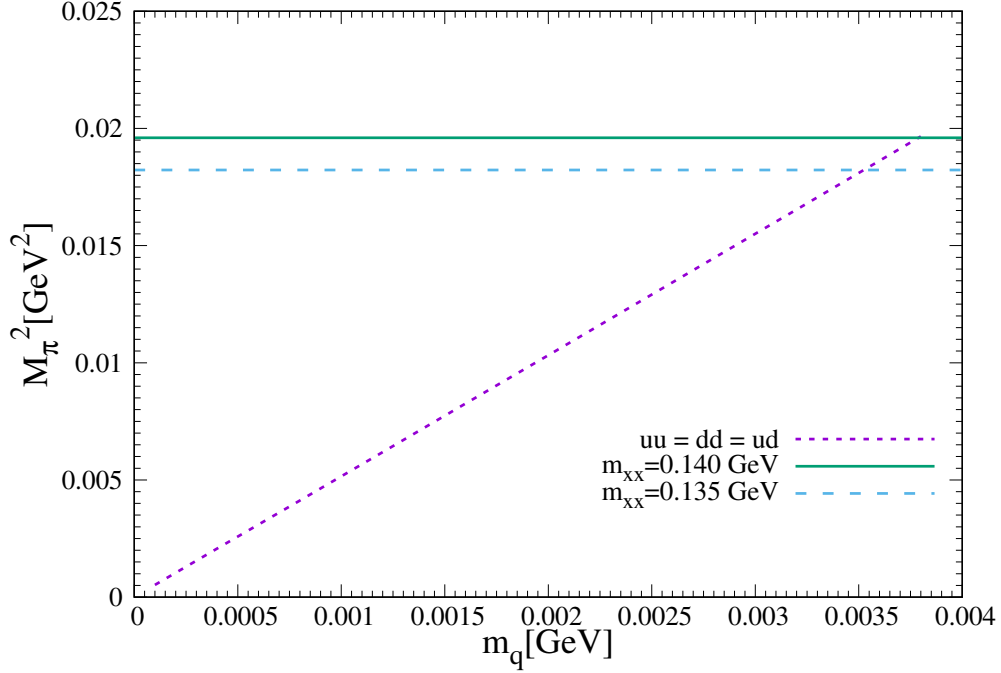


Figure 3.4: The Gell-Mann - Oakes - Renner relation shows the relation between quark mass and the squared pion mass. The two horizontal lines mark the physical pion masses at  $(0.135 \text{ GeV})^2$  and  $(0.140 \text{ GeV})^2$ . We use this plot mainly to show results for a range of different quark masses at a time while keeping the pion mass splitting in our mind.

## 3.2 Modeling QED

We identified the two manifestations of isospin symmetry. Our next step is to modify our calculations to handle quark mass and charge separately. Almost trivial is the change in mass, since the current mass is explicitly treated in the equations. Inserting different values for  $m_u$  and  $m_d$  immediately lifts the content degeneration of  $\pi^\pm$ ,  $\pi^0$ ,  $K^\pm$ ,  $K^0$ ,  $\rho^\pm$  and  $\rho^0$ . This step leads to the matter of defining particles by their quark content. Previously, a pseudoscalar containing two quarks of mass  $m_{u\bar{d}}$  automatically was labeled pion. The same was true for kaons ( $m_{u\bar{d}}$  and  $m_s$ ) and in the case of vector mesons rhos (two times  $m_{u\bar{d}}$  again). Now, the content of  $\pi^\pm(ud)$ ,  $K^\pm(us)$ ,  $K^0(ds)$  and  $\rho^\pm(ud)$  are clear, while the neutral states are left to be constructed from  $uu$  and  $dd$  states. We use the quadratic average [52, 53]

$$M_{\pi^0}^2 = \frac{M_{uu,PS}^2 + M_{dd,PS}^2}{2} \quad (3.11)$$

$$M_{\rho^0}^2 = \frac{M_{uu,V}^2 + M_{dd,V}^2}{2}, \quad (3.12)$$

where  $M_{uu,PS/V}$  and  $M_{dd,PS/V}$  are the pure bound state masses for pseudoscalar and vector quantum numbers. An alternative naive approach would be a linear averaging

$$M_{\pi^0} = \frac{M_{uu,PS} + M_{dd,PS}}{2} \quad (3.13)$$

$$M_{\rho^0} = \frac{M_{uu,V} + M_{dd,V}}{2}. \quad (3.14)$$

Comparing these two and possible other way to construct neutral mesons might be an interesting topic for future work.

We mention or show some intermediate results and plots in this section to motivate further modifications to the model. The discussion will follow in section 3.3, when we are able to relate the findings to a coherent picture.

We tested pairs of  $m_u$  and  $m_d$  constraining the choice so that the resulting charged pion is physical,  $M_{\pi^\pm} = 140$  MeV, while the mass of the neutral pion is open to change. We find that the effects of the different mass in the quark and the bound state seem to cancel each other, leading to the same result for both pions,  $M_{\pi^\pm} = M_{\pi^0}$ . This renders the pion splitting a perfect opportunity to fix the parameters of our expanded model. The results for the mass pairs are listed in table II in section 3.3.

The more interesting parts are the electromagnetic corrections. We implement these by adding an electromagnetic self energy to the quark. The first try was a naive photon exchange with tree-level vertices. Corrections to the photon itself can be neglected, since we know that lepton-loops are of a higher electromagnetic order. Quark-loops were found to be even further subleading, which we know from hadronic vacuum polarization considerations. Instead, analogue to the quark self energy, one quark-photon vertex should be fully dressed with all twelve tensor structures. To be able to solve the quark, we keep the leading structure corresponding to the bare vertex  $\gamma^\mu$  and drop the rest, similar to the truncation of the quark-gluon vertex. The advantage of this procedure is that we arrive at a term simply added to the effective interaction  $\alpha_{eff}$ . Photon and gluon are both transverse exchange bosons and thus have the same tensor structure. Constructing a new effective interaction  $\tilde{\alpha}_{eff}$  of the form

$$\tilde{\alpha}_{eff} = \alpha_{eff}^{QCD} + \alpha_{eff}^{QED}, \quad (3.15)$$

we identify

$$\alpha_{eff}^{QED} = \alpha_0 Q_q^2 \tilde{Z}_{QED}(q^2), \quad (3.16)$$

where  $Q_q^2$  is the squared charge of the quark.  $\alpha_0$  denotes the electromagnetic coupling at zero momentum transfer.  $\tilde{Z}_{QED}$  corresponds to the dressing related to the

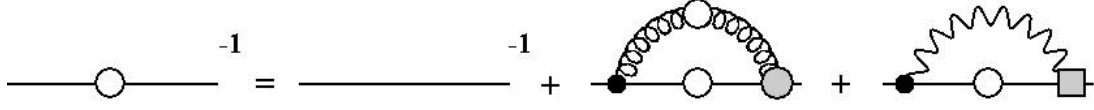


Figure 3.5: The QED extended DSE for the quark propagator. Additionally to bare quark and hadronic self energy, we add an electromagnetic self energy. The squared vertex denotes the truncated and modeled quark-photon vertex.

vertex structure  $\gamma^\mu$ . Our truncation dictates that it can only depend on the squared gluon momentum. In figure 3.5 we show the new modified DSE with electromagnetic exchange diagram and truncated vertex. We mark this vertex with a square.

Now we need to find a meaningful description of the dressing  $\tilde{Z}_{QED}$ . The full quark-photon vertex obeys a Ward-Takahashi identity derived from the  $U(1)$  gauge symmetry of QED

$$iP^\mu \Gamma_\mu(P, p) = S^{-1}(p_+) - S^{-1}(p_-). \quad (3.17)$$

The vertex can be separated in a transverse part  $\Gamma_\mu^T$ , where the WTI yields the form

$$P^\mu \Gamma_\mu^T = 0, \quad (3.18)$$

and the fixed non-transverse part  $\Gamma_\mu^{NT}$ , explicitly related to the quark dressing functions. The resulting vertex, called Ball-Chiu vertex [54] consists of four of the twelve tensor structures. It reads

$$\begin{aligned} \Gamma_\mu^{BC} = & \gamma_\mu \frac{A(p_+^2) + A(p_-^2)}{2} + 2\not{p}p_\mu \frac{A(p_+^2) - A(p_-^2)}{p_+^2 - p_-^2} \\ & - 2ip_\mu \frac{B(p_+^2) - B(p_-^2)}{p_+^2 - p_-^2}. \end{aligned} \quad (3.19)$$

We see that the tree-level vertex  $\gamma_\mu$  is accompanied by the term

$$\Gamma^{1BC} = \frac{A(p_+^2) + A(p_-^2)}{2}, \quad (3.20)$$

but our truncation only allows dependences on the squared photon momentum  $q^2$ . Instead, we use an alternative ansatz, which satisfies fundamental requirements as multiplicative renormalisability and correct perturbative behavior [55]. We effectively substitute the quark  $A$  functions

$$\frac{A(p_+^2) + A(p_-^2)}{2} \simeq A(q^2). \quad (3.21)$$

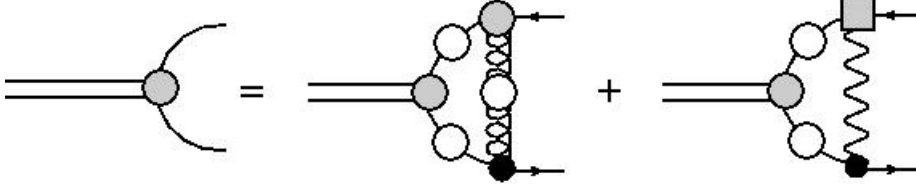


Figure 3.6: Meson bound state BSE with an additional photon exchange diagram. The squared vertex is the same truncated modeled vertex we introduced in the quark.

We now define the dressing as,

$$\tilde{Z}_{QED}(q^2) = f_m \frac{A_1(q^2) + A_2(q^2)}{2}, \quad (3.22)$$

where  $f_m$  was introduced to compensate interaction strength relative to the QCD part lost by dropping non-dominant tensor structures.  $A_1$  and  $A_2$  are the dressing functions of the two quarks in the vertex. For the DSE, it will always be the same quark, but in the meson BSE we have to average two potentially different flavors.

We fix  $f_m$  by using the measured pion mass splitting. As mentioned before, in the case of the pions, basically the full splitting is a result of electromagnetic interaction. Knowing this, we extend our model to incorporate QED in the meson BSE while keeping the quark mass degenerated, for now leaving only  $f_m$  as an open parameter.

The natural way to extend the meson BSE is, analogue to what we did to the quark DSE, add a photon exchange diagram mirroring the existing gluon exchange. Contrary to the DSE, we now have to deal with one quark and one antiquark. Previously there was no difference in the treatment, but introducing a charge changed this and has to be accounted for. Phenomenologically, we know that a bound state constituted by charged particles should have higher mass compared to the neutral state, so we implement the additional diagram in an appropriate way. We show the BSE diagram equation with the new contribution in figure 3.6.

Mathematically, the change is the same modification to  $\alpha_{eff}$ . Only this time with a minus sign relative to the quark implementation, to treat the antiquark charge, which is the anti charge  $Q_{\bar{q}} = -Q_q$  of its quark partner. These two minus signs cancel and let us pretend that the antiquark is a quark. Now we calculate the meson with the same modification as the quark, exchanging the squared quark charge  $Q_q^2$  by the product of the charges of the two quarks  $Q_q^2 \rightarrow Q_1 \cdot Q_2$ .

This setup allows us to solve the system of  $u$  and  $d$  quark and  $uu$ ,  $dd$  and  $ud$  bound states for different  $f_m$ . We know that the quark mass splitting contributions to the

pion mass splitting is of negligible size. We also found that in the probed range of  $f_m = 1 - 1.4$  the effects in DSE and BSE cancel for the pure states  $uu$  and  $dd$ , while the mixed state  $ud$  and thus  $\Delta M_\pi^2 = M_{\pi^\pm}^2 - M_{\pi^0}^2$  changes. Adjusting  $f_m$  so that  $M_{\pi^\pm}$  and  $M_{\pi^0}$  both have their physical value for a degenerated mass of the  $u$  and  $d$  quark defines the model. We scan through  $u$  masses and find their  $d$  partner to produce physical pions. These pairs, listed in table VII in the next section, are candidates that need to be verified by the kaon mass splitting. To do so, we keep both masses  $M_{K^\pm}$  and  $M_{K^0}$  constant at their (rounded) measured values and try to find an  $s$  quark mass producing these results with an  $u, d$  candidate pair. The masses we find are

$$m_u = 2.45 \text{ MeV} \quad m_d = 4.61 \text{ MeV} \quad m_s = 84.88 \text{ MeV} \quad (3.23)$$

with a model fixed at

$$f_m = 1.3. \quad (3.24)$$

A consistency check, calculating all pseudoscalar masses we used to find these values in the model, gives

$$\begin{aligned} m_{\pi^\pm} &= 140 \text{ MeV} & m_{K^\pm} &= 494 \text{ MeV} \\ m_{\pi^0} &= 135 \text{ MeV} & m_{K^0} &= 498 \text{ MeV} \end{aligned} \quad (3.25)$$

This is the full setting we use in the thesis. Before we consider applications, we use the next section to show the explicit plots and results that took us all the way to find the models parameter set.

## 3.3 Discussion of the results

In this section we take a close look at our actual results. The baseline to our meson results are the masses shown in table I.

The first step we described was lifting current mass degeneracy. When we calculate the charged pion, we can keep the mass fixed at the physical value  $M_{\pi^\pm} = 140$  MeV. Running the code with the  $u$  mass as input, we vary the  $d$  mass until the system converges. The pairs found were then used to calculate the neutral pion mass. Table II shows the quark mass pairs and the corresponding bound state masses. We see essentially no difference between the fixed  $M_{\pi^\pm}$  and the calculated  $M_{\pi^0}$ . In the quark dressing functions, we can see the influence of higher current mass directly, since it is basically the only distinction between any quarks right now. The modified quark masses does not seem to have enough impact to significantly change the meson masses, however. The mass  $M_{\pi^0}$ , being subject to one raised and one lowered mass compared to an averaged quark stays the same as  $M_{\pi^\pm}$ .

| $m_u$ | $m_d$ | $M_{uu}$ | $M_{dd}$ | $M_{\pi^0}$ |
|-------|-------|----------|----------|-------------|
| 0.50  | 7.10  | 50.5     | 191.7    | 140.20      |
| 1.00  | 6.60  | 71.7     | 184.8    | 140.15      |
| 1.50  | 6.10  | 87.8     | 177.6    | 140.10      |
| 2.00  | 5.60  | 101.4    | 170.1    | 140.05      |
| 2.50  | 5.10  | 113.5    | 162.3    | 140.03      |
| 3.00  | 4.61  | 124.3    | 154.1    | 140.01      |
| 3.50  | 4.10  | 134.4    | 145.5    | 140.03      |
| 4.00  | 3.60  | 143.7    | 136.3    | 140.03      |

Table II: Results for lifted quark mass degeneracy. Fixing  $u$  and  $\pi^\pm$  mass lets us find corresponding  $d$  masses. These pairs produce  $uu$  and  $dd$  bound states which we quadratically average to  $\pi^0$  masses. We see that no matter how huge the quark mass splitting is, the recombined  $\pi^0$  mass stays unchanged. All values are listed in MeV.

Considering other approaches, this is not surprising. Calculations of the electromagnetic corrections to the pion splitting explain almost the whole observed mass difference and can be calculated by the Cottingham formula [56, 57]. Additionally, lattice calculations yielded similar results, which can be found for example in a review of low energy particle physics of the FLAG group [58].

The electromagnetic extension lets us investigate some more interesting cases. As explained in the last section, we extended the quark DSE and meson BSE separately. This allowed us to further analyze the cancellation of contributions stemming from the quark versus the meson equation. The additional quark self energy behaves as a raised mass. The quark charge always appears squared, so the flavor only determines the extent of said raise. In the meson BSE, we have to distinguish between quark and antiquark and adjust the sign of the extension accordingly, so that the overall charged bound state gains additional mass.

Our first tests were performed using a bare photon vertex in the calculations. We made use of our previous findings and keep the masses  $m_u = m_d = m_q$  degenerated, since their impact on the pion splitting is negligible anyway. Now we calculated systems of  $m_q$ ,  $M_{uu}$ ,  $M_{dd}$ ,  $M_{\pi^0}$  and  $M_{\pi^\pm}$ . Even with the same mass,  $u$  and  $d$  quark and thus their bound states are set apart by their charge. The influence of quark and meson equation can be tested by turning the extra diagrams on or off. Test cases were: QED only in the quark, QED only in the meson, and QED in both equations. We show the results in GMOR like plots in figures 3.7 to 3.9.

| $m_q$ | $M_{uu}$ | $M_{dd}$ | $M_{\pi^0}$ | $M_{\pi^\pm}$ |
|-------|----------|----------|-------------|---------------|
| 0.1   | 33.93    | 25.82    | 30.15       | 30.00         |
| 0.4   | 51.77    | 47.01    | 49.45       | 49.50         |
| 0.8   | 68.90    | 65.31    | 67.13       | 67.13         |
| 1.2   | 82.57    | 79.54    | 81.07       | 81.07         |
| 1.6   | 94.29    | 91.60    | 92.95       | 92.95         |
| 2.0   | 104.71   | 102.27   | 103.50      | 103.50        |
| 2.4   | 114.20   | 111.93   | 113.07      | 113.07        |
| 2.8   | 122.97   | 120.83   | 121.91      | 121.91        |
| 3.2   | 131.17   | 129.13   | 130.15      | 130.15        |
| 3.8   | 142.59   | 140.68   | 141.64      | 141.64        |

Table III: Calculated results for bound states of interest in MeV using a bare vertex in the QED expansion implemented only in the quark DSE. The quark mass is degenerated,  $u$  and  $d$  quark are defined by their respective charge. All bound states acquire additional mass,  $u$  content always gaining more by the higher  $u$  charge. The final pion masses are degenerated,  $u$  and  $d$  changes cancel each other.

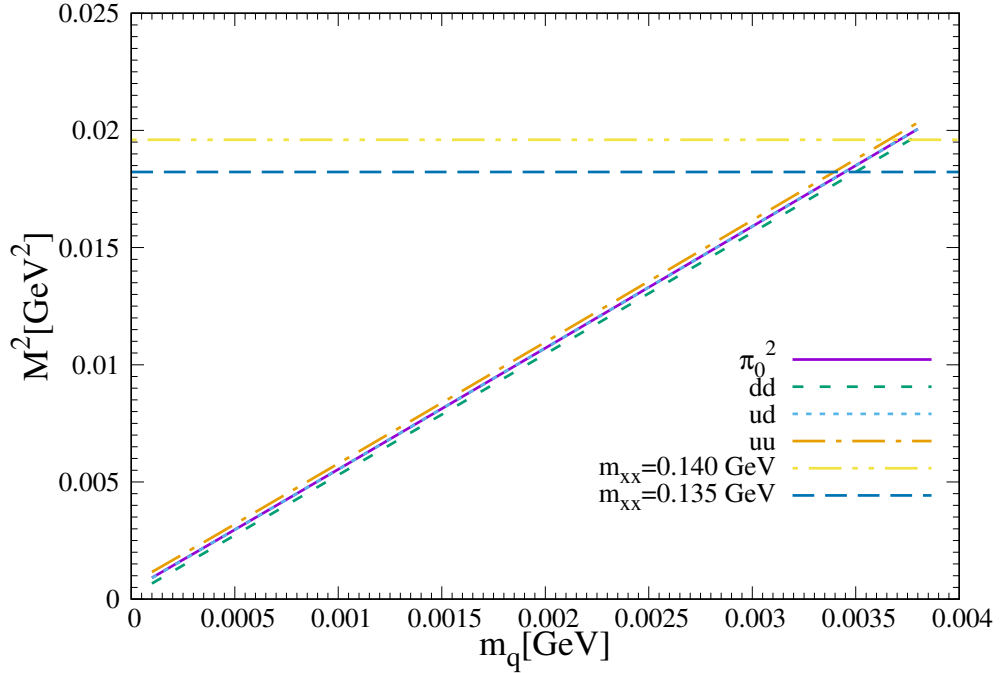


Figure 3.7: GMOR plot for  $M_{uu}^2$ ,  $M_{dd}^2$ ,  $M_{\pi^0}^2$  and  $M_{\pi^\pm}^2$  with QED extension in the quark DSE using a bare quark-photon vertex. Corresponding data is listed in table III.



| $m_q$ | $M_{uu}$ | $M_{dd}$ | $M_{\pi^0}$ | $M_{\pi^\pm}$ |
|-------|----------|----------|-------------|---------------|
| 0.1   | -        | 18.85    | -           | 28.68         |
| 0.4   | 37.91    | 43.59    | 40.85       | 48.76         |
| 0.8   | 58.95    | 62.83    | 60.92       | 66.48         |
| 1.2   | 74.37    | 77.50    | 75.95       | 80.50         |
| 1.6   | 87.11    | 89.81    | 88.47       | 92.43         |
| 2.0   | 98.23    | 100.65   | 99.45       | 103.00        |
| 2.4   | 108.23   | 110.44   | 109.34      | 112.60        |
| 2.8   | 117.38   | 119.43   | 118.41      | 121.44        |
| 3.2   | 125.89   | 127.81   | 126.85      | 129.70        |
| 3.8   | 137.67   | 139.45   | 138.56      | 141.19        |

Table IV: Calculated results for bound states of interest in MeV using a bare vertex in the QED expansion implemented only in the meson BSE. Bound states where quark and antiquark have opposite charge experience a lowered mass ( $uu$ ,  $dd$ ).  $M_{\pi^\pm}$ , with quark and antiquark of similar charge gains mass, giving us the first significant pion mass splitting. Our BSE implementation becomes unstable for very low masses, so we did not reach convergence for  $M_{uu}$  with  $m_q = 0.1$ .

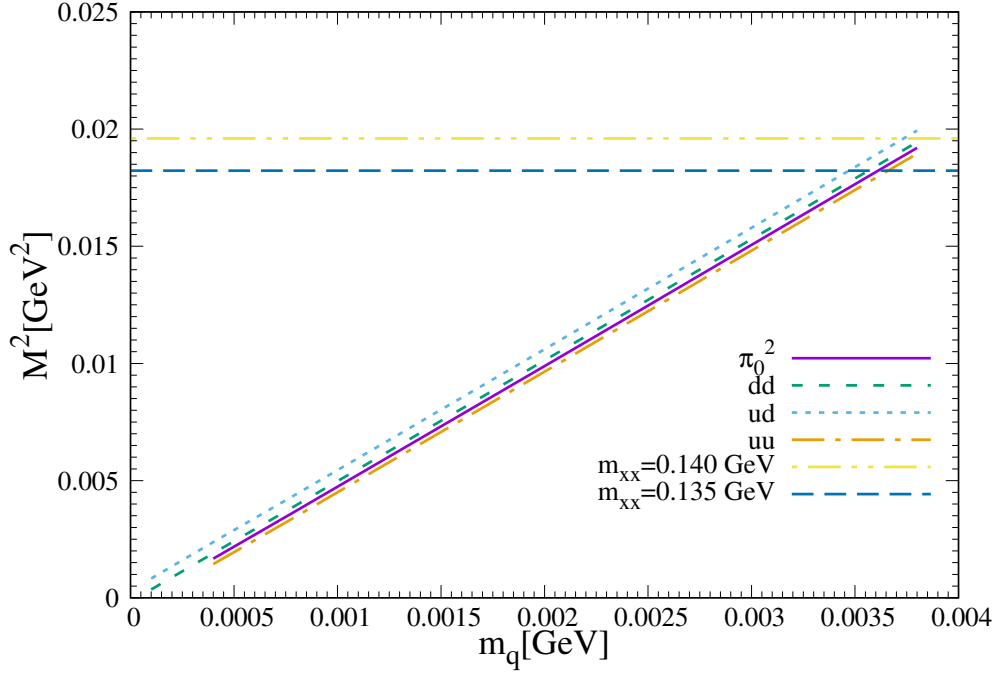


Figure 3.8: GMOR plot for  $M_{uu}^2$ ,  $M_{dd}^2$ ,  $M_{\pi^0}^2$  and  $M_{\pi^\pm}^2$  with QED extension in the meson BSE using a bare quark-photon vertex. We see the first relevant pion mass splitting. Corresponding date is listed in table IV.

The data shows the expected effects of the QED extensions. Implementing the charge in the DSE effectively raises the quark mass. The raised quark mass raises the bound state mass for all calculated states. As seen in table III, the effect varies depending on the quark content.  $Q_u$  is twice as big as  $Q_d$ , thus the gain is highest for  $M_{uu}$ . An interesting observation is, that the averaged effect in  $M_{\pi^0}$  is exactly the same as in  $M_{\pi^\pm}$ .

In the case of only an extended BSE, we have to keep in mind how we set up the model. We implemented the extension in a specific way, to ensure that an overall charged meson has higher mass than a neutral particle. The absolute value of the charge product determines how big the effect is. Figuratively speaking, the neutral pion averaged over the loss and the charged pion averages the potential gain from one  $u$  and one  $d$  quark charge. Results are listed in table IV.

Table V combines both extensions. All states have raised mass from the DSE, but at the same time neutral final states lose mass from the BSE. Only  $M_{\pi^\pm}$  gets its mass raised by both effects. Notable is, that the two effects negate each other and give us  $M_{uu} = M_{dd} = M_{\pi^0}$ .

In general, calculating with quark masses producing pions around the physical pion masses is enough, but we wanted to show two things. First, the quadratic dependency keeps satisfied by the extension, which is reassuring. Secondly, the mass splitting is independent of the quark mass. Intuitively this is natural, since electromagnetic corrections to a bound state mass can be seen as a purely electromagnetic cloud in-

| $m_q$ | $M_{uu}$ | $M_{dd}$ | $M_{\pi^0}$ | $M_{\pi^\pm}$ |
|-------|----------|----------|-------------|---------------|
| 0.1   | 22.59    | 22.60    | 22.60       | 35.05         |
| 0.4   | 45.38    | 45.34    | 45.36       | 52.50         |
| 0.8   | 64.17    | 64.10    | 64.13       | 69.43         |
| 1.2   | 78.64    | 78.54    | 78.59       | 83.00         |
| 1.6   | 90.84    | 90.73    | 90.79       | 94.65         |
| 2.0   | 101.61   | 101.48   | 101.54      | 105.03        |
| 2.4   | 111.35   | 111.21   | 111.13      | 114.49        |
| 2.8   | 120.31   | 120.16   | 120.24      | 123.22        |
| 3.2   | 128.66   | 128.50   | 128.58      | 131.39        |
| 3.8   | 140.28   | 140.09   | 140.18      | 142.79        |

Table V: Calculated results for bound states of interest in MeV using a bare vertex in the QED expansion implemented in both the quark DSE and the meson BSE. The two effects of DSE and BSE cancel almost perfectly for the pure states  $M_{uu}$  and  $M_{dd}$  and thus also for  $M_{\pi^0}$ . The charged pion picks up raised mass from both effects.

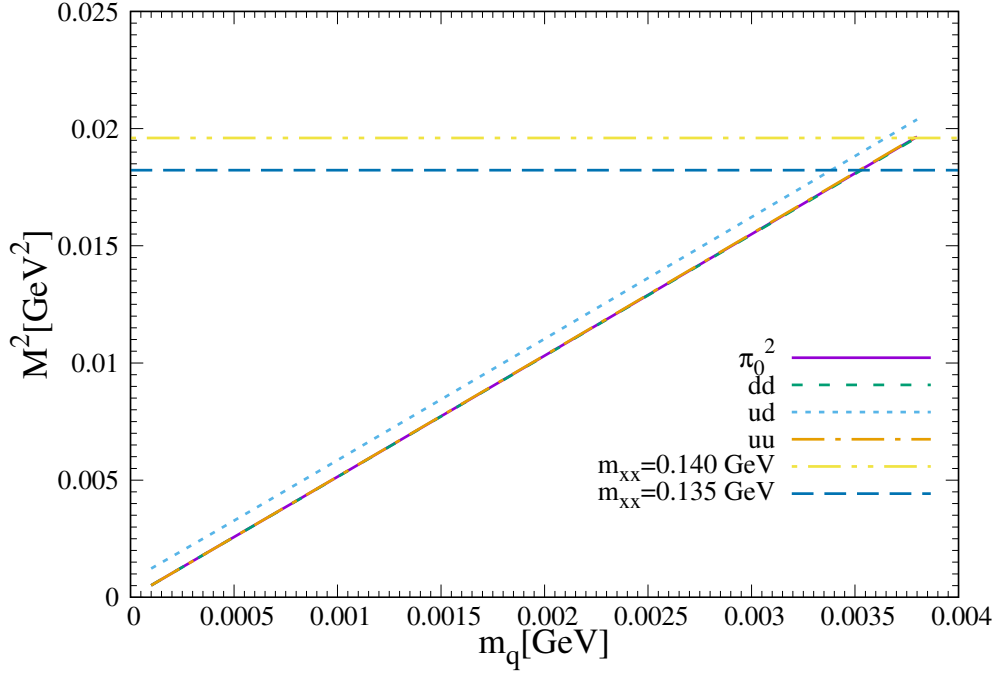


Figure 3.9: GMOR plot for  $M_{uu}^2$ ,  $M_{dd}^2$ ,  $M_{\pi^0}^2$  and  $M_{\pi^\pm}^2$  with QED extension in the quark DSE and meson BSE using a bare quark-photon vertex. The difference between the neutral states is numerically negligible. Masses are generally raised, but the splitting originating from the BSE part is the same as before. Corresponding date is listed in table V.

interacting with the particle. This cloud cannot see anything except the charge of the particle and thus needs to behave as it does in our results. QCD corrections to the photon vertex expose this line of thinking as naive, but so far, these were neglected.

The splitting we observe is not enough to explain the experimentally observed masses. We already know that by omitting structures of the photon vertex, significant information is lost. Using the 1BC like vertex ansatz with equation 3.22, dependent on the squared gluon momentum, is the best truncation we are able to implement. Our calculations showed that it restores some of the lost strength, but an additional compensation in form of a strength factor  $f_m$  was needed to fit the model to the measured splitting. An unexpected finding was that  $M_{uu} = M_{dd}$  was still valid for all tested interaction strengths. Even with a nontrivial vertex, contributions from DSE and BSE canceled each other within the scope of numerical accuracy. The influence of the vertex can be understood as a quark dressing dependent effective charge. The

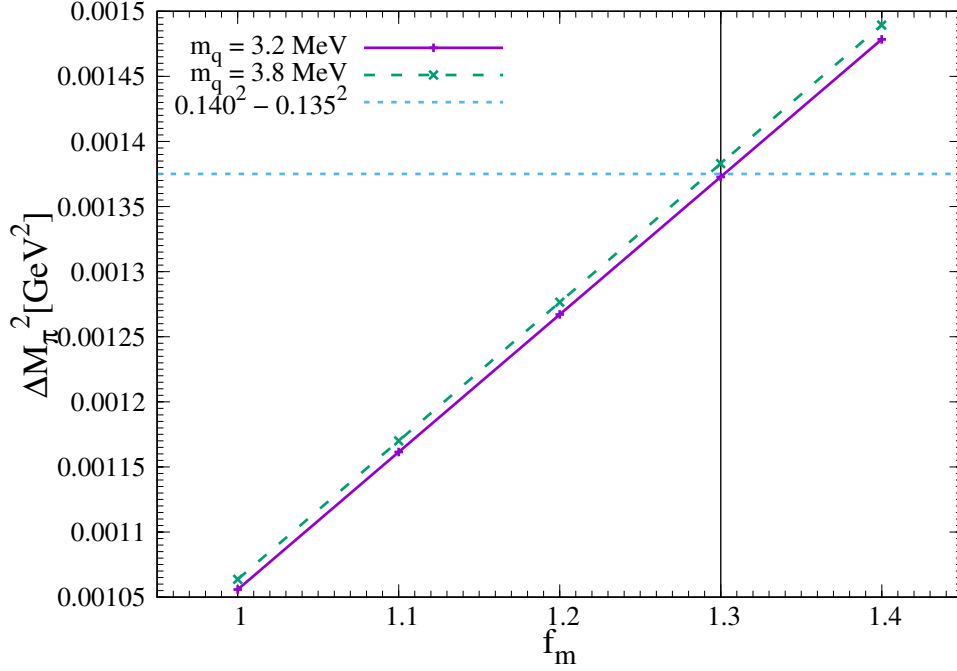


Figure 3.10: Dependence of the pion mass splitting  $\Delta M_\pi^2$  of the strength factor  $f_m$ . The linear behavior easily allows us to identify  $f_m = 1.3$  as the necessary model to reproduce physical pion splitting.

effective charge however will always be bigger than the bare charge, amplifying the influence of DSE and BSE described previously. Since the behavior mirrors the case of the bare vertex otherwise, we do not show additional plots for DSE and BSE extensions separately.

The increase of  $\Delta M_\pi^2 = M_{\pi^\pm}^2 - M_{\pi^0}^2$  with the strength factor  $f_m$  was found to be almost linear (see figure 3.10). In the quark mass region of physical pions, the required splitting could be constructed with

$$f_m = 1.3. \quad (3.26)$$

With an  $A$  dressing dependent vertex, the  $m_q$  independence of the splitting was lost. As seen in figure 3.11, the effect is tiny, so using a value of the general physical region of  $m_q$  is good enough. Table VI lists results for  $f_m = 1.3$  in the region of physical pion masses.

| $m_q$ | $M_{uu}$ | $M_{dd}$ | $M_{\pi^0}$ | $M_{\pi^\pm}$ |
|-------|----------|----------|-------------|---------------|
| 2.4   | 111.53   | 111.38   | 111.45      | 117.39        |
| 2.8   | 120.51   | 120.33   | 120.42      | 125.96        |
| 3.2   | 128.87   | 128.68   | 128.77      | 134.00        |
| 3.8   | 140.50   | 140.28   | 140.39      | 145.23        |

Table VI: Bound state results for QED extension in both DSE and BSE with a 1BC inspired vertex model in MeV. We show results for the strength factor  $f_m$  which produces the observed physical pion mass splitting.

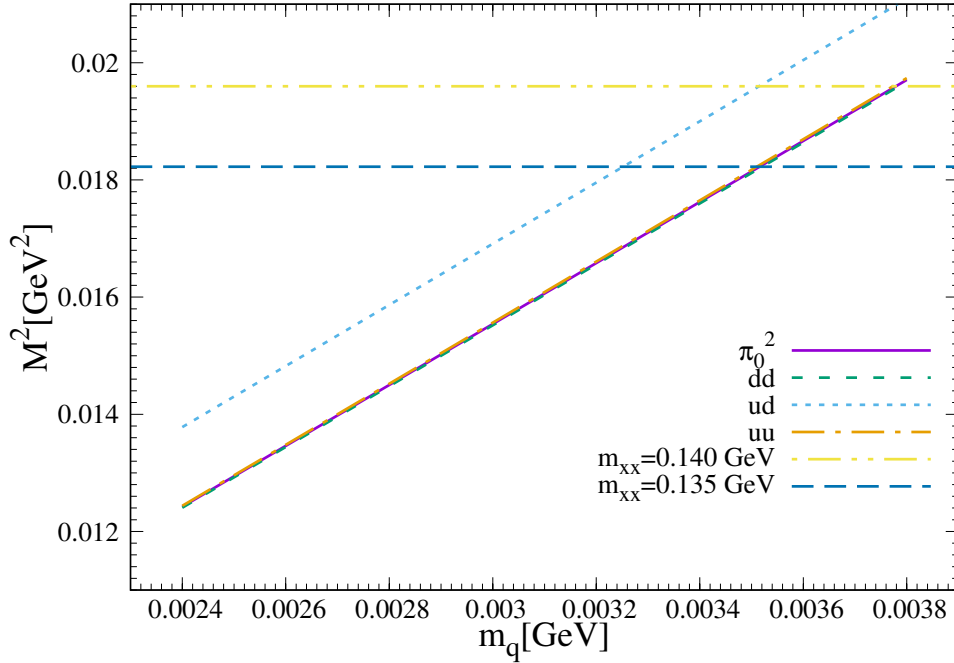


Figure 3.11: Results for  $M_{uu}^2$ ,  $M_{dd}^2$ ,  $M_{\pi^0}^2$  and  $M_{\pi^\pm}^2$  with QED extension in the quark DSE and meson BSE using a 1BC inspired quark-photon vertex. The pion mass splitting is not necessarily independent of  $m_q$  anymore, but we see that the impact in the region of physical pion masses is negligible.

With fixed QED extension, we can get our focus back on the quark mass degeneracy. While the interaction strength ensured the proper mass splitting, we were able to concentrate on the charged pion to find potential  $u$  and  $d$  quark masses to produce physical pions. The requirement was that we wanted to produce physical kaons

| $m_u$ | $m_d$ | $m_s(K^0)$ | $m_s(K^\pm)$ |
|-------|-------|------------|--------------|
| 1.50  | 5.56  | 84.01      | 85.75        |
| 2.00  | 5.06  | 84.47      | 85.29        |
| 2.25  | 4.81  | 84.69      | 85.07        |
| 2.45  | 4.61  | 84.88      | 84.89        |
| 2.50  | 4.56  | 84.92      | 84.84        |
| 2.55  | 4.51  | 84.97      | 84.80        |
| 2.65  | 4.42  | 85.05      | 84.70        |
| 2.75  | 4.31  | 85.14      | 84.61        |
| 3.00  | 4.06  | 85.37      | 84.39        |
| 3.50  | 3.56  | 85.83      | 83.93        |

Table VII: Potential  $u$ ,  $d$  pairs which produce physical pions. Each pair requires different  $s$  quark masses to produce physical kaon masses. The pair that uses the same  $s$  quark for both  $K^\pm$  and  $K^0$  is the pair we use for our model. All masses are listed in MeV.

simultaneously. We used these masses to find  $s$  quarks that solve the meson BSE for physical kaons, where each  $u$ ,  $d$  pair produces one  $s$  quark per kaon. A pair where both  $s$  quarks coincide fixes the model. In table VII, we show the  $u$ ,  $d$  masses and the two  $s$  quarks generated by  $K^\pm$  and  $K^0$ .

The final masses we find this way, which we already pointed out in equation 3.23, are

$$m_u = 2.45 \text{ MeV} \quad m_d = 4.61 \text{ MeV} \quad m_s = 84.88 \text{ MeV}. \quad (3.27)$$

While the model is to some extent phenomenologically motivated in its implementation, this set is surprisingly reasonable. The  $u$  and  $d$  quark mass splitting is of the correct order, while the  $s$  quark varies only slightly compared to standard values in RL-MT calculations. As a reminder, the masses were found by enforcing the physical light meson masses and setting the correct pion splitting.

With the model parameters determined, we wanted to look into the effects on the vector meson channel. This channel is supposedly most important in the calculation of the hadronic vacuum polarization, which is the main motivation for this work. We compared the influence of our modifications to the baseline results  $M_\rho = 745.31$  MeV and  $M_\phi = 1075.36$  MeV.

Test calculations we performed were done with the model masses without QED extension realized by  $f_m = 0$ , the standard masses used for the baseline results with QED extension, and the full model. The results for relevant bound states are listed in table VIII. In the first column, we see how the split quark masses lower  $M_{uu}$  and raise  $M_{dd}$  compared to the baseline masses. The recombined neutral rho mass

|                | $m_u = 2.45$<br>$m_d = 4.61$<br>$m_s = 84.88$<br>$f_m = 0$ | $m_u = 3.7$<br>$m_d = 3.7$<br>$m_s = 85.0$<br>$f_m = 1.3$ | $m_u = 2.45$<br>$m_d = 4.61$<br>$m_s = 84.88$<br>$f_m = 1.3$ |
|----------------|--|---|--|
| $M_{uu}$       | 738.95   | 745.82  | 739.43   |
| $M_{dd}$       | 749.89   | 745.43  | 750.02   |
| $M_{\rho^0}$   | 744.44   | 745.63  | 744.74   |
| $M_{\rho^\pm}$ | 744.46   | 746.12  | 745.26   |
| $M_\phi$       | 1074.93  | 1075.83   | 1075.41  |

Table VIII: Bound state masses in the vector channel. All test cases produce a splitting less than 0.6 MeV for the rho mesons. The phi meson also only changes marginally. Considering the general numerical accuracy, changes in the vector channel are basically nonexistent.

however does not show any splitting to the charged  $\rho$ , similar to the pseudoscalar channel without electromagnetic model extension. The  $\phi$  only experiences a slightly lowered  $s$  mass, so  $M_\phi$  is lowered minimally.

Second column shows the impact of the electromagnetic component in DSE and BSE simultaneously. Compared to the pion,  $\rho$  and  $\phi$  are significantly less influenced by the extra terms. Changes around 0.5 MeV in the  $\phi$ , and a  $\rho$  mass splitting of the same magnitude in a system that is numerically less stable than its pseudoscalar counterpart cannot give any deeper insights.

The last column shows results for the full model. In the pion case, we were able to cover the full 5 MeV splitting, but here we see almost no change in splitting and  $\phi$  mass. The changes in  $M_{uu}$  and  $M_{dd}$  for different  $u$  and  $d$  mass in column one and three are way lower than what the pseudoscalar channel would produce. The vector bound states generate their mass to a higher extend by their structure and depend less on the current masses. Interpreting our model in a way of effectively changing current masses in DSE and BSE with a defined prescription, does not have a huge impact in the more 'stagnant' vector masses.

It is essential to consider the fact, that the averaging of 'pure' vector channel bound states does not cover the well known problem of  $\rho - \omega$  mixing [59]. The analysis present in this thesis restricts itself in an analogous way of looking at the  $\rho$  to the pion and does not incorporate any corrections in this direction. The reproduction of the measured nonexistent  $\rho$  mass splitting can in this light only be seen as a hint in the right direction and not much more.

It is hard to define a proper error to results calculated in our framework. We know that the for HVP most important physics lie in the vector mesons, and thus want to set up a quark mass set, which allows us to compute  $\rho$  and  $\phi$ . Fixing the masses

$$M_\rho = 775 \text{ MeV} \quad M_\phi = 1020 \text{ MeV}, \quad (3.28)$$

with averaged  $u$  and  $d$  mass and without QED corrections, we find

$$m_{\bar{u}d} = 9.74 \text{ MeV} \quad m_s = 69.54 \text{ MeV}. \quad (3.29)$$

Because of the above explained uncertainties in the rho channel, we cannot set up the model directly by fixing it to the vector channel. Instead we take the deviation between our model calculations to calculations using this quark set as our systematic error.



## 4 Application to the anomalous magnetic moment of leptons

Chapter 4 summarizes the first application of our isospin symmetry breaking model. We motivate the general interest in the anomalous magnetic moment of leptons  $a_l$  and give an overview over the development of our understanding of this particular observable, with separate focus on theoretical and experimental extraction. Next we explain the functional approach to the hadronic vacuum polarization function. Finally we single out the changes our model induces, and conclude with a discussion of our results for  $\mu$  and  $\tau$  lepton.

### 4.1 Magnetic moments

As mentioned in the introduction, our group already spend some effort and achieved respectable results concerning the analysis of anomalous magnetic moments of the muon  $a_\mu$  [25–29]. The hadronic vacuum polarization in particular was shown to give results comparable to dispersive calculations, while being derived from first principle calculations. The used polarization function  $\Pi_R$  is, in this attribute, superior to most other approaches, since we do not need to separate high and low energy QCD contributions. One logical step to extend our approach is to combine the existing HVP calculations with our isospin symmetry breaking model from chapter 3.

The main reason why the leptonic anomalous magnetic moment is considered a ‘smoking gun’ observable is the fact that it includes all given interactions of the standard model. By logical extension, any new physics following a similar quantum field description, would show up as well. These contributions are calculated separately and by this distinction, it was possible to determine  $a_l$  as one of the most precisely calculated property of particle physics. At the same time, extensive efforts on the experimental side made this precision necessary to compete with measured results [60]. Even now, a new experiment for the muon anomalous magnetic moment is on its way at J-PARC [61]. The traditional setup is also still used at Fermilab to further reinforce and improve the experimental value [62].

The following general overview over history, standard model results and experimental progress are mainly based on refs. [63, 64]. While we might quote some specific references, not all original sources will be listed here, especially ones that are old or hard to access. The affected references can be found in the listed summaries in this case.

As for most leptonic observables, the first experimental approach was targeted at the electron. In 1924, the Stern-Gerlach experiment was the first step in the measurement of magnetic moments of leptons. Shortly after Goudsmith and Uhlenbeck [65] postulated the electron magnetic dipole moment as

$$\mu_e = \frac{e}{2m_e}, \quad (4.1)$$

following the study of the anomalous Zeemann effect. While Pauli left the gyromagnetic factor  $g$  in

$$\vec{\mu}_l = g_l \frac{e}{2m_l} \vec{S} \quad (4.2)$$

as a free parameter, Dirac presented the treatment of the relativistic electron with  $g_e^{theo} = 2$  in 1928 [66]. Six years later Kinster and Houston measured  $g_e^{exp} = 2$  and validated Diracs prediction. Continuous improvement in the experimental measurement techniques [67] and the growing theoretical understanding of QED renormalization led to the agreement that the magnetic moment actually contains an anomalous part. The famous lepton flavor independent Schwinger result from 1948 [68]

$$a_l = \frac{\alpha}{2\pi}, \quad (4.3)$$

which contributes around 99% of the electrons anomalous magnetic moment, was at the time one of the most influential results, sparking interest and acceptance of quantum field theories in the physicists community. With the refinement of measurement, the theoretical calculations soon became dependent on the inclusion of weak and strong contributions to achieve comparable precision [60]. While the electromagnetic parts strongly dominate the overall results, other parts were no longer negligible, especially in the case of the muon. This was analyzed first by Berestetskii in 1956, who reported an enhanced sensitivity for anomalous magnetic moments. His finding was a proportionality

$$\delta a_l \sim \frac{m_l^2}{M^2}, \quad (4.4)$$

where  $\delta a_l$  is the contribution to  $a_l$  of a quantum fluctuation with the given scale  $M$  of the fluctuations theory. In the case of e.g. the weak interaction, this would be the W-boson mass, for the strong interaction the scale  $\Lambda_{QCD}$ . This statement has two important implications. It shows that the muon has much bigger contributions

of non-QED theories than the electron, since the mass ratio

$$\left(\frac{m_\mu}{m_e}\right)^2 \simeq 4 \cdot 10^4 \quad (4.5)$$

strongly favors the muon. As a side note, any measurement of the  $\tau$  lepton would outshine the muon, but by nature of the  $\tau$  lifetime no reliable results have been agreed upon yet. The second implication is the obvious decrease of impact in the result with growing scale  $M$ . This means that we have an exceptionally precise tool to investigate 'new physics' in the direct proximity of the standard model.

Theoretical and experimental results for the muon are

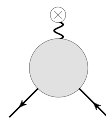
$$a_\mu^{SM} = 116591827(64) \cdot 10^{-11}, \quad (4.6)$$

$$a_\mu^{Exp} = 116592089(63) \cdot 10^{-11}. \quad (4.7)$$

An overview of different sources can be found in [63]. The general confidence in the respective results and correlating errors poses an inquiring situation: using the results that were calculated and measured for the muon, we find deviations well out of the error range. It shows that research in the field of the anomalous magnetic moment of the muon is far from being concluded. In the next two sections we give compilation of theoretical and experimental approaches to the anomalous magnetic moments of leptons with focus on the muon..

## 4.2 Standard model contributions to $g - 2$

The information of the magnetic moment is found in the lepton-lepton-photon vertex  $\Gamma_l^\mu$ . It is defined by



$$= \bar{u}(p') \Gamma_\alpha u(p) = \bar{u}(p') \left[ \gamma_\alpha F_1(k^2) + \frac{i}{2m_\mu} \sigma_{\alpha\beta} q^\beta F_2(k^2) \right] u(p) \quad (4.8)$$

$F_1$  and  $F_2$  are the Dirac and Pauli formfactors, the  $\bar{u}$ ,  $u$  spinors describe the scattered on-shell muon and  $q$  the external photon momentum which will eventually be set to zero. Also, we use the notation  $\sigma_{\alpha\beta} = i[\gamma_\alpha, \gamma_\beta]/2$ .

We consider the matrix element

$$\mathcal{M} = e \bar{u}(p') \Gamma_\mu u(p) A_\mu^{cl}(\vec{k}), \quad (4.9)$$

with the momentum representation of the classical background field

$$A_\mu^{cl}(x) = \left(0, \vec{A}(\vec{x})\right). \quad (4.10)$$

In the nonrelativistic limit the lepton spinors can be approximated by

$$u(p) \simeq \sqrt{m_l} \begin{pmatrix} (1 - \vec{p} \cdot \vec{\sigma}/2m_l) \xi \\ (1 + \vec{p} \cdot \vec{\sigma}/2m_l) \xi \end{pmatrix}. \quad (4.11)$$

With vanishing photon momentum  $q \rightarrow 0$  and by expressing the photon via a magnetic field

$$B^k(\vec{k}) = -i\epsilon^{ijk}k^i A^j(\vec{k}), \quad (4.12)$$

we get the following result

$$\mathcal{M} = 2m_l \frac{e}{m_l} [F_1(0) + F_2(0)] \left\langle \frac{\sigma^k}{2} \right\rangle B^k(\vec{k}), \quad (4.13)$$

which identifies as a Born approximation with potential

$$V(\vec{x}) = -\langle \vec{\mu} \rangle \vec{B}(\vec{x}), \quad (4.14)$$

$$\langle \vec{\mu} \rangle = \frac{e}{m_l} [F_1(0) + F_2(0)] \left\langle \frac{\vec{\sigma}}{2} \right\rangle. \quad (4.15)$$

Charge renormalization additionally gives us

$$F_1(0) = 1, \quad (4.16)$$

which lets us postulate

$$g_l = 2[F_1(0) + F_2(0)] = 2 + 2F_2(0), \quad (4.17)$$

leading finally to

$$a_l = F_2(0) = \frac{g_l - 2}{2}. \quad (4.18)$$

More detailed derivations can be found in most quantum field theory text books, e.g. in [69].

While it is possible to project  $F_2$  directly by applying

$$P_\mu = \frac{m_l^2}{q^2(q^2 + 4m_l^2)} \gamma_\mu - i \frac{m_l(2m_l^2 - q^2)}{q^2(q^2 + m^2)^2} (p + p')_\mu \quad (4.19)$$

to  $\Gamma_\mu$  and taking the limit  $q \rightarrow 0$  afterwards, the numerical treatment is quite involved. A more elegant alternative [70, 71] uses a linear expansion of the vertex in the photon momentum  $q$

$$\Gamma_\mu(P, q) \simeq \Gamma_\mu(P, 0) + q^\nu \frac{\partial}{\partial q^\nu} \Gamma_\mu(P, q) \Big|_{q=0}. \quad (4.20)$$

This allows to directly work in the limit  $q \rightarrow 0$  and gives

$$a_l = \frac{1}{48m_l} \text{Tr} \left[ (\not{p} + m_l) [\gamma_\alpha, \gamma_\beta] (\not{p} + m_l) \left( \frac{\partial}{\partial q_\alpha} \Gamma_\beta \right) \right] \Big|_{q=0}. \quad (4.21)$$

The standard model result for  $a_l$  is now constructed by identifying, calculating, and adding up contributions from vertex corrections. By far dominant is the electromagnetic correction. It includes the Schwinger result 4.3 mentioned before. Because of the perturbative nature of QED, its terms are understood, but by no means trivial to calculate. Starting from second order,  $a_l$  includes lepton mass dependent contributions, breaking lepton universality

$$a_e \neq a_\mu \neq a_\tau. \quad (4.22)$$

The Schwinger result represents lowest order in only one diagram, but second order already consists of nine parts. We will from now on focus on  $a_\mu$  with explicit numbers. The systematics however do not change for electron and  $\tau$ . Diagrams 7, 8 and 9 in figure 4.2 show the QED photon vacuum polarization which is the equivalent of the hadronic vacuum polarization we are interested in. The number of relevant diagrams grows fast. Order three consists of 72 terms while fourth order already includes around a thousand contributions. In 2012 even fifth order has been calculated [72]. Table I shows the different contributions of QED by loop order.

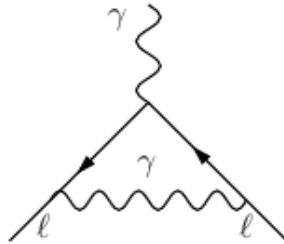


Figure 4.1: The Schwinger result dominates corrections to the magnetic moment of leptons. Its origin is the QED one loop correction diagram to the muon vertex.

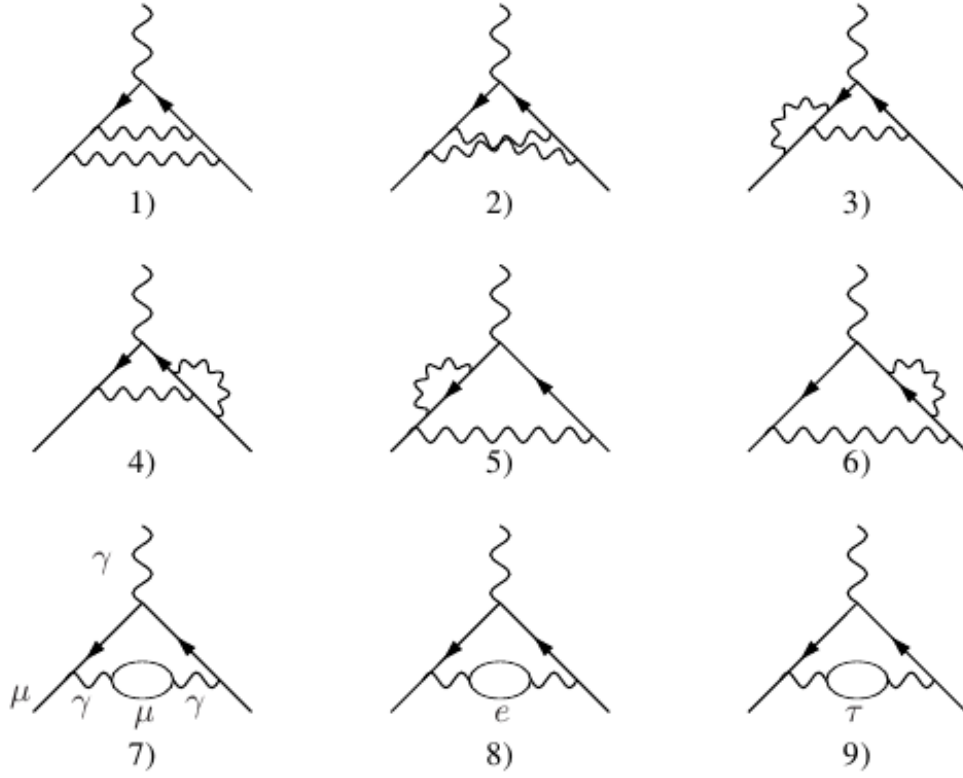


Figure 4.2: The complexity of QED loop diagrams is perturbatively under control, but the sheer amount of diagrams rises fast. Second order already has nine diagrams, including vacuum polarization diagrams.

| Loop order | $a_{\mu}^{QED}[\cdot 10^{11}]$        |
|------------|---------------------------------------|
| 2          | 413217.621(14)                        |
| 3          | 30141.902(1)                          |
| 4          | 380.807(25)                           |
| 5          | $753.29(1.04)(\alpha/\pi)^5 \simeq 5$ |

Table I: Results for the QED contributions to  $a_{\mu}$  up to fifth order loop diagrams.

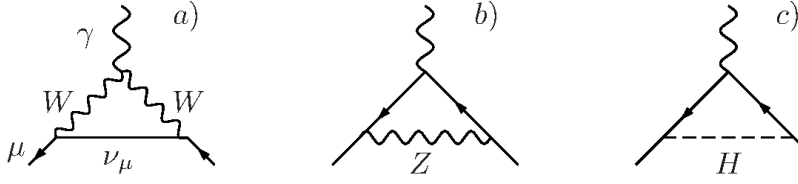


Figure 4.3: Weak correction diagrams can also be treated perturbatively. The overall yield is so small that less than full third order is enough to satisfy accuracy. This figure shows first order diagrams.

Weak interaction diagrams are also perturbative. Thus, calculations are again straight forward, but we already know because of Berestetskii that any results are suppressed by the heavier scale. Considering this, it is not surprising that already second order, complemented by dominant third order diagrams are enough to arrive at an acceptable precision. Figure 4.3 shows the lowest order weak diagrams. The weak contribution to  $a_\mu$  is given by [73]

$$a_\mu^{weak} = 153.5(1.0) \cdot 10^{-11}. \quad (4.23)$$

Finally arriving at QCD, we find two distinct sorts of contributions shown in figure 4.4. The dominant part is the hadronic vacuum polarization. We will discuss it later in in this chapter. For now, it is important to know that this part can be related to experimental data [74, 75]. With growing experimental precision, the result  $a_\mu^{HVP}$  will as well get more reliable.

The second part is the hadronic light-by-light (HLbL) scattering. While our group did a considerable amount of research on this topic, the present thesis does not focus on it. We will therefor restrict ourself to general considerations. Light-by-light is

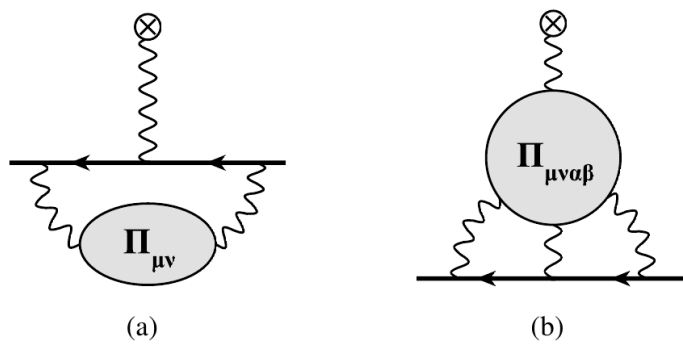


Figure 4.4: QCD contributions consist of hadronic vacuum polarization (a) and hadronic light-by-light scattering (b).

| QCD     | $a_\mu[\cdot 10^{11}]$ |
|---------|------------------------|
| HVP, LO | 6949.1(58.2)           |
| HVP, HO | -98.4(1.0)             |
| HLbL    | 105(26)                |

Table II: Results for the hadronic vacuum and hadronic light-by-light contributions to  $a_\mu$ , as agreed upon in the community. Although the error in the HVP result is the largest in calculating  $a_\mu$ , the connection to experimental data will eventually resolve the uncertainty. HLbL on the other hand, is a topic of continuous discussion.

contrary to HVP not yet relateable to experimental data. Thus, the accepted present value was calculated using effective field theories giving rise to an error driven by estimates. The debatable treatment of this contribution and its error marks it as an interesting field of study right now. The results for hadronic contributions separated in HVP leading order, higher order and HLbL [74, 76] are listed in table II.

The standard model result for  $a_\mu$  is the sum of all present contributions. We arrive at

$$a_\mu^{SM} = 116591827(64) \cdot 10^{-11}, \quad (4.24)$$

where the error is dominated by hadronic contributions.

### 4.3 Experiment

The main requirement, and also problem in earlier experimental approaches to measure the anomalous magnetic moment of the muon, is the production of polarized muons. Parity violation in pion decays [77] however lead to the current predominant experimental setup to measure  $a_\mu$ .

At CERN, measurements of the anomalous magnetic moment were conducted with the CERN cyclotron (1958-1962), and a muon storage ring from 1962 until 1968 [78]. The measurements with the storage ring produced a deviation  $1.7 \sigma$  between theory and experiment, which made it necessary to include higher QED loop orders in the calculation. A second muon storage ring at CERN [79], operation during 1969-1976, was precise enough to measure the first hadronic contribution to  $a_\mu$ , the hadronic vacuum polarization. With the experiment E821 at Brookhaven [80], running until 2003, the precision reached a point where even weak interaction contributions needed to be included. The Brookhaven ring is nowadays used at Fermilab for the experiment E989 [62] which aims to further reduce uncertainties.



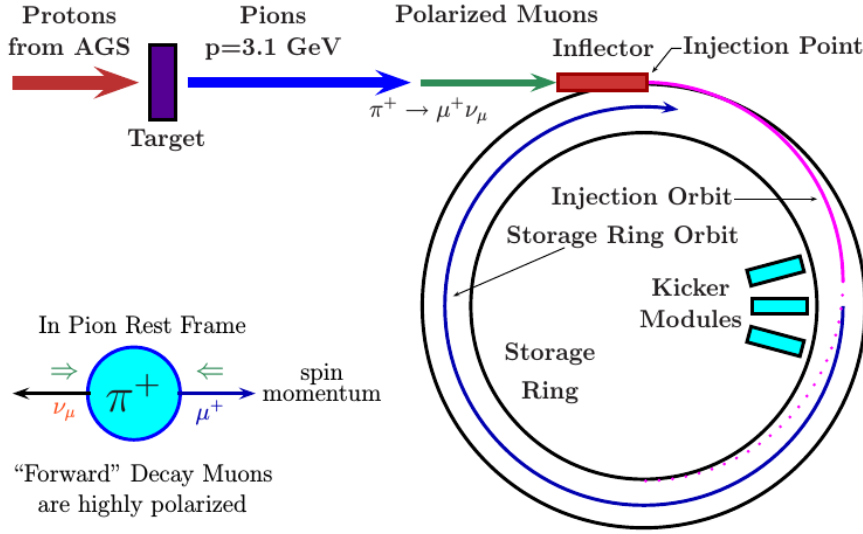


Figure 4.5: Schematic view of experiments of the type of the former Brookhaven experiment E821 and the new Fermilab experiment E989. The anomalous magnetic moment of the muons in the storage ring can be detected by measuring decay products after numerous circulations in the ring. [63]

The concept of this type of experiment is based in spin precession. To begin with, protons hitting a target produce pions. These pions decay weak by

$$\pi \rightarrow \mu + \nu_\mu, \quad (4.25)$$

where the fixed neutrino handedness ensures a highly polarized muon beam. Figure 4.5 is taken from [63] and shows the experimental setup of the Brookhaven experiment schematically. The trapped muons now move in a relativistic cyclotron motion with frequency

$$\omega_c = \frac{eB}{m_\mu \gamma}, \quad (4.26)$$

$\gamma$  being the Lorentz factor. The spin axis however changes according to the Larmor precession. The angular frequency of the spin is given by

$$\omega_s = \frac{eB}{m_\mu \gamma} + a_\mu \frac{eB}{m_\mu}, \quad (4.27)$$

which gives us direct access to the anomalous magnetic moment via

$$\omega_a = \omega_s - \omega_c. \quad (4.28)$$

In reality this setup required an additional electric field to focus muons in the storage ring. This field adds an extra term to the frequency

$$\vec{\omega}_a = \frac{e}{m_\mu} \left( a_\mu \vec{B} - \left[ a_\mu - \frac{1}{\gamma^2 - 1} \right] \vec{v} \times \vec{E} \right), \quad (4.29)$$

where  $\vec{v}$  is the muon velocity. Specific tuning of the beam energy to  $E_{mag} = \gamma m \simeq 3.098$  GeV allows to completely negate the term depending on the field  $\vec{E}$ . This “magic Energy” is the basis of the described type of experiment.

The resulting relativistic muons have the additional advantage that their lifetime in the ring drastically rises. While the muon typically decays after  $\simeq 2.2 \mu\text{s}$ , it can survive  $\simeq 64.4 \mu\text{s}$  in the ring. This allows many laps making for a more precise measurement. The decay finally happens as

$$\mu \rightarrow e + \nu_\mu + \nu_e, \quad (4.30)$$

with the corresponding neutrino and anti-neutrino. The direction of positron emission is strongly determined by the muon spin direction. This correlation is used to extract  $\omega_a$  from the counting rate, distribution and energy of the emitted positrons. More detailed informations and additional sources can be found in [62, 63, 80].

Using this method the experimentally extracted value for  $a_\mu$  is

$$a_\mu^{Exp} = 116592089(63) \cdot 10^{-11}. \quad (4.31)$$

The only known disadvantage of the explained treatment is also quite obvious. By using the “magic Energy”, any experimental setup uses the exact same energy. This could theoretically allow systematic uncertainties the different experiments share and thus cannot be compensated by cross checking.

To provide such a cross check, an alternative setup was proposed and is currently build and tested in Japan at J-PARC as experiment E34 [61]. Again, a proton beam is used on a target to produce muons. In this case, interest lies on so called surface muons, which are produced by decaying pions at rest. These muons are collected to form  $Mu$ , an electron-muon muonium. With the help of lasers, thermal muons can be extracted from excited  $Mu$  states, retaining sufficient polarization to proceed. These muons are re-accelerated to an energy of 300 MeV and injected into a storage ring. The main difference to conventional experiments is that these muons have a very small transverse momentum dispersion. Effectively, the need for an electric focusing field vanishes and the restriction of using  $E_{mag}$  is lifted.

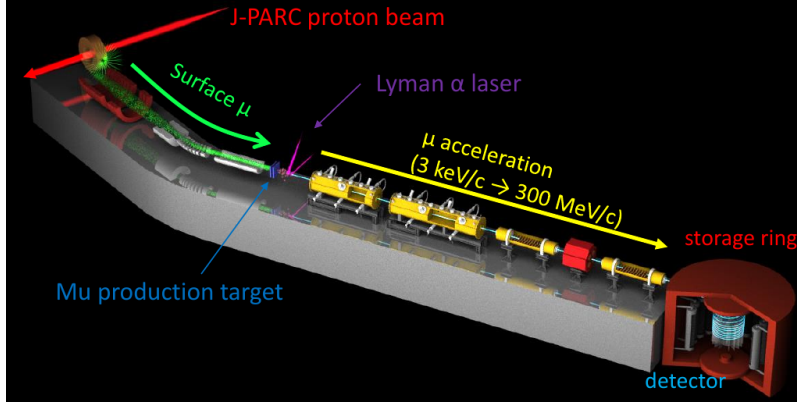


Figure 4.6: Schematic view of the setup of J-PARC experiment E34, [61]. The new experimental setup is a great chance to allow an analysis of potentially unknown systematic errors in the commonly used measurement method.

Some notes concerning efficiency should be mentioned. Compared to fast muons, polarization is significantly lower. At the same time lower energy in the storage ring directly correlates with muon lifetime and thus with spin precession. On the other hand, lower energy allows a smaller diameter of the ring. Overall, already the promise of the alternative systematics for measurements of anomalous magnetic moments makes pursuing this approach worthwhile. A schematic view of the experiment is shown in figure 4.6, which was published in [61].

## 4.4 Hadronic vacuum polarization

The QCD contribution we concentrate on is the hadronic vacuum polarization. To get this specific part, we need to calculate the  $a_l$  projection of the diagram depicted in figure 4.7, respectively solve the equation

$$a_l^{HVP} = \frac{\alpha}{\pi} \int_0^1 dx (1-x) \left[ -e^2 \Pi_R \left( \frac{x^2}{1-x} m_l \right) \right] \quad (4.32)$$

where  $\Pi_R$  is the renormalized hadronic polarization function [81]. This object contains the physical behavior and is the focal point of the application of our model.

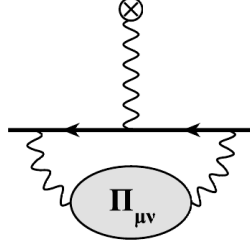


Figure 4.7: The hadronic vacuum polarization contribution to  $a_\mu$  is the main object of interest in this thesis. The hadronic corrections to the photon propagator in turn modify the photon correction to the muon vertex.

In the DSE/BSE approach, the hadronic polarization function is defined by the hadronic self energy term of the photon DSE. We start from the QED Lagrangian

$$\mathcal{L}_{QED} = Z_\psi^{QED} \bar{\psi} (\not{\partial} + m) \psi + ie Z_{\psi A}^{QED} \bar{\psi} \not{A} \psi + Z_A^{QED} \frac{F_{\mu\nu} F_{\mu\nu}}{4} \quad (4.33)$$

where  $A_\mu$  is now the  $U(1)$  gauge field of a photon and  $F^{\mu\nu}$  the field strength tensor. As a part of the standard model, QED is renormalizable. Commonly the scale is chosen to ensure physical electron mass and electric charge at the physical pole masses.

$$m(\mu^2 = m_e^2) = m_{phys} \quad e(\mu^2 = 0) = e_{phys}. \quad (4.34)$$

The photon DSE is constructed in an analogous way to the quark DSE, using  $\mathcal{L}_{QED}$  and applying functional derivatives with respect to the photon field. In euclidean momentum space the inverse dressed photon propagator can be evaluated by

$$D_{\mu\nu}^{-1}(p) = Z_A^{QED} p^2 \left( \delta_{\mu\nu} - \frac{p_\mu p_\nu}{p^2} \right) + \Pi_{\mu\nu}(p) \quad (4.35)$$

diagrammatically shown in figure 4.8, with the explicit expression

$$\Pi_{\mu\nu}(p) = -e Z_2 \int_q \frac{dq}{(2\pi)^4} \text{Tr}[S(q_+) \gamma_\mu S(q_-) \Gamma_\nu(p, q)] \quad (4.36)$$

for the hadronic self energy tensor ( $q_\pm = q \pm p/2$ ).  $Z_2$  is the quark renormalization. At this point we need to insert quark propagators  $S(q_\pm)$ , as well as the quark-photon vertex  $\Gamma_\mu(p, q)$ , which we already introduced in chapter 3. As with the quark, in theory this equation is exact. By the insertion of our quark propagators and the calculation of the photon vertex, we inherit truncations applied earlier. Figure 4.9 shows the self energy tensor in rainbow-ladder truncation. The self energy is calculated for each quark flavor separately and joined in the end with its appropriate charge factors.

$$\overset{-1}{\text{wavy line}} = \overset{-1}{\text{wavy line}} + \text{quark loop diagram}$$

Figure 4.8: The photon DSE gives us access to the hadronic photon self energy. In the DSE/BSE framework, the self energy consists of a dressed quark loop coupled to the photon with one bare and one fully dressed quark-photon vertex.

$$\begin{aligned} \text{wavy line} \text{ with } \Pi_{\mu\nu} &= \text{quark loop with gluon exchange} + \text{quark loop with gluon exchange} \\ &+ \text{quark loop with gluon exchange} + \dots \\ &= \text{quark loop diagram} \end{aligned}$$

Figure 4.9: The hadronic vacuum polarization of the photon is the self energy part of the photon DSE. In Rainbow-Ladder truncation, it can be understood as a summation of all planar diagrams emitting and absorbing gluons in the quark loop. Gluon exchanges that go across the vertex contribute to the dressed vertex, all other exchanges to the two dressed quarks.

Before we can concentrate on the extraction of the renormalized vacuum function from the tensor, we need to explain the photon vertex. The general setup was already mentioned in chapter 3. We have again twelve dressing functions  $\Gamma_i$  with corresponding tensor structures  $B_i^\mu$  separated in  $L_i^\mu$  and  $T_i^\mu$ , spanning a basis of the space

$$\{\gamma_\mu, p_\mu, q_\mu\} \otimes \{\mathbb{1}, \not{p}, \not{q}, [\not{p}, \not{q}]\}. \quad (4.37)$$

We use this separated basis system allowing to identify the four Ball-Chiu structures as  $L_1^\mu$  to  $L_4^\mu$  while the elements  $T_i^\mu$  cover the transversal part of the vertex. Explicitly the basis reads [82]

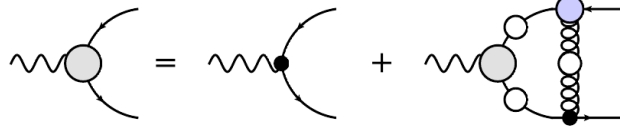


Figure 4.10: The quark-photon vertex BSE generates a system of twelve coupled integral equations. Compared to the meson BSE, additionally to the increased size of the system, also an inhomogeneous bare vertex term is included. This term allows to numerically solve it straight forward with a fixed point iteration.

$$L_1^\mu = \gamma^\mu$$

$$L_2^\mu = -(\not{p}_1 + \not{p}_2)(p_1 + p_2)^\mu$$

$$L_3^\mu = -i(p_1 + p_2)^\mu$$

$$L_4^\mu = -i\sigma^{\mu\nu}(p_1 + p_2)_\nu$$

$$T_1^\mu = i(p_1^\mu(p_2 \cdot p_3) - p_2^\mu(p_1 \cdot p_3))$$

$$T_2^\mu = (p_1^\mu(p_2 \cdot p_3) - p_2^\mu(p_1 \cdot p_3))(\not{p}_1 + \not{p}_2)$$

$$T_3^\mu = \not{p}_3 p_3^\mu - p_3^2 \gamma^\mu$$

$$T_4^\mu = -i(p_3^2 \sigma^{\mu\nu}(p_1 + p_2)_\nu + 2p_3^\mu \sigma_{\lambda\nu} p_1^\lambda p_2^\nu)$$

$$T_5^\mu = i\sigma^{\mu\nu} p_{3\nu}$$

$$T_6^\mu = (p_1^2 - p_2^2) \gamma^\mu + (p_1 + p_2)^\mu \not{p}_3$$

$$T_7^\mu = \frac{i}{2}(p_1^2 - p_2^2) \left( (\not{p}_1 + \not{p}_2) \gamma^\mu - (p_1 + p_2)^\mu \right) - i(p_1 + p_2)^\mu \sigma_{\lambda\nu} p_2^\lambda p_1^\nu$$

$$T_8^\mu = -\gamma^\mu \sigma_{\lambda\nu} p_2^\lambda p_1^\nu - \not{p}_2 p_1^\mu + \not{p}_1 p_2^\mu$$

Here we use the notation  $p_3 = p_2 - p_1$  and  $\sigma_{\mu\nu} = (\gamma_\mu \gamma_\nu - \gamma_\nu \gamma_\mu)/2$ , as written in the reference. The vertex equation itself is a Bethe-Salpeter equation, given by

$$\Gamma^\mu(p, q) = Z_2 \gamma^\mu - \frac{4}{3} Z_2^2 \int \frac{dk}{(2\pi)^4} D^{\alpha\nu}(q - k) \gamma^\alpha S(q_+) \Gamma^\mu(p, k) S(q_-) \gamma^\nu, \quad (4.38)$$

where we went back to our previous notation for momenta. Mathematically, it is a vector meson BSE with an inhomogeneous bare vertex term. Numerically, solving

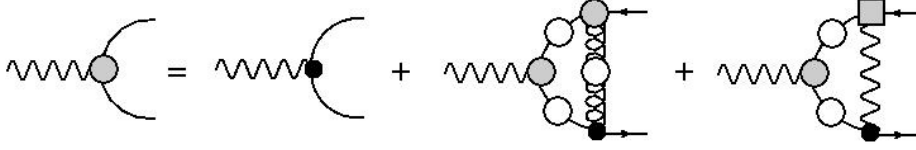


Figure 4.11: The QED model extension to the DSE/BSE framework needs to be implemented in the vector BSE as well. The procedure is analogous as in the meson BSE before, by adding the photon correction diagram with 1BC motivated model vertex.

for the dressings  $\Gamma_i$  is even more straight forward, since the inhomogeneous term renders the eigenvalue convergence obsolete. The projectors  $P_i^\mu$  needed to extract the separate dressings satisfy

$$\text{Tr}[P_i^\mu B_j^\mu] = \delta_{ij}. \quad (4.39)$$

They were calculated analogous to the projectors in the meson BSE using standard linear algebra methods.

As before, we insert the extended model at the effective interaction level, treating the antiquark-quark content as in the case of the mesons.

This gives us everything we need to work on the polarization tensor  $\Pi_{\mu\nu}$ . As a photon self energy, it is transversal. Thus we are able to define a unique dressing function  $\Pi$ , by writing

$$\Pi_{\mu\nu}(p) = \left( \delta_{\mu\nu} - \frac{p_\mu p_\nu}{p^2} \right) p^2 \Pi(p^2). \quad (4.40)$$

The transverse projector

$$P_\Pi^{\mu\nu}(p) = \frac{1}{3} \left( \delta_{\mu\nu} - \frac{p_\mu p_\nu}{p^2} \right) \quad (4.41)$$

applied to equation 4.36 gives us an explicit result for

$$p^2 \Pi(p^2) = P_\Pi^{\mu\nu}(p) \Pi_{\mu\nu}(p^2). \quad (4.42)$$

The vacuum polarization itself is logarithmically divergent and needs to be renormalized by adjusting renormalization constants in the photon DSE. Additionally, the numerical treatment of calculating in hyperspherical coordinates, and introducing a hard cutoff for the squared momentum, generates another unphysical quadratic cutoff dependency. This artifact can be projected out using a Brown-Pennington projector [83]. Alternatively we can subtract it at  $p^2 = 0$ . While we use the latter, both methods were tested and agree very well. The explicit treatment is as follows. First we take care of the quadratic term by subtracting the whole diagram at  $p^2 = 0$ .

$$[p^2 \Pi(p^2)]_R = [p^2 \Pi(p^2)] - [p^2 \Pi(p^2)]|_{p^2=0} \quad (4.43)$$

Since the logarithmic divergence is unaffected by this subtraction, we need to apply a second renormalization

$$\Pi_R(p^2) = \frac{[p^2 \Pi(p^2)]_R}{p^2} - \left[ \frac{[p^2 \Pi(p^2)]_R}{p^2} \right]_{p^2=0} \quad (4.44)$$

The resulting polarization function is finally cutoff independent. Further explanations and considerations concerning numerical stability can be found in [50].

## 4.5 Results in HVP

Joining all previously explained parts together we have a way to implement our electromagnetic extension to the hadronic vacuum polarization by inserting the modified quark propagators and photon vertex. Otherwise the calculation proceeds as before.

All in all, we performed HVP calculations with five distinguished set. We wanted to investigate the influence of quark masses and electromagnetic corrections, and estimate a model uncertainty. The results we refer to from now on, are listed in table III for muon and IV for the  $\tau$  lepton.

First, we take a look at our baseline set, standard masses without QED in the effective coupling. Compared to previous calculations, e.g. in [50], our results are generally  $\sim 7\%$  lower, which is in the estimated error range. As we noted in chapter 2, we use different quark systematics, and slightly different MT parameter, which generate these deviations.

| $a_\mu^{HVP}$ in $\cdot 10^{-10}$ | $u$   | $d$   | $s$  | $c$  | $b$ (disc.) | $\Sigma$ |
|-----------------------------------|-------|-------|------|------|-------------|----------|
| DSE/BSE error                     | 455.5 | 113.9 | 57.7 | 11.0 | 0.0         | 638.1    |
| DSE/BSE base                      | 501.3 | 125.3 | 50.4 | 11.0 | 0.0         | 687.7    |
| DSE/BSE base <sup>QED</sup>       | 500.3 | 125.2 | 50.4 | 10.8 | 0.0         | 686.4    |
| DSE/BSE $\Delta m_q$              | 511.8 | 123.4 | 50.5 | 11.0 | 0.0         | 696.3    |
| DSE/BSE $\Delta m_q^{QED}$        | 510.9 | 123.4 | 50.4 | 10.8 | 0.0         | 695.1    |
| BMWC                              | 674.5 | -     | 53.7 | 14.7 | -12.8       | 711.0    |
| Disp.                             | -     | -     | -    | -    | -           | 694.9    |

Table III: HVP contributions to the anomalous magnetic moment of the  $\mu$  lepton. Lattice data was published by the Budapest-Marseille-Wuppertal collaboration [84]. It does not add up, since numerous corrections were administered to the final result, which are not listed for separate quark masses. In the  $b$  quark column, we list disconnected lattice contributions, that need to be subtracted. The dispersion relation result was taken from [63].



Our error set, which we set up to reproduce correct  $\rho$  and  $\phi$  masses in chapter 3, gives lower results for  $u$  and  $d$ , and higher for  $s$  flavor. The summed up result for muon leads to  $\sim 8 - 9\%$  difference to the full model. We use this to assume a model uncertainty of the order of 10% for our absolute values  $a_\mu^{HVP}$ .

When we turn on QED without quark mass splitting, we find corrections less than 0.2% to  $u, d$  and the overall result. The same can be observed when we compare results for our model masses with and without electromagnetic contributions. Since we already found similar behavior in the vector meson channel, these results are a confirmation of our previous reflections.

There is no need to discuss quark mass splitting effects isolated, since QED seems to be negligible in HVP anyway. When we compare our baseline results to the full model, we find isospin corrections of  $\sim 1.9\%$  for the  $u$  flavor,  $\sim 1.5\%$  for  $d$ , and  $\sim 1.1\%$  for the full result.

Our results show a reasonable agreement with lattice data [84]. The lattice result does not add up in the result tables, since corrections that were administered to the full result were not listed for the flavor separate values. Some of these corrections try to compensate for isospin symmetry breaking effects. There are some, in ref. [84] labeled 'exploratory' investigations [85], which report isospin effects of 1.5(4)% from direct calculations. They perform a rescaling, reducing current mass dependency in  $a_\mu$ , which gives a final result of 0.4(4)% for isospin symmetry breaking. These first results and our calculations agree in the order of the effects and in the dominant role of quark mass splitting as the reason for observed effects. We take this as a hint, that our phenomenological model covers most of the relevant physics concerning hadronic vacuum polarization.

The agreement with dispersive results is excellent [63]. Considering the estimated error in our calculations, we have to admit that this precision is probably a lucky coincidence, though.

The  $\tau$  lepton hadronic vacuum polarization has not been calculated in the DSE/BSE framework yet. We find  $\sim 0.5\%$  isospin corrections to the full result. Our agreement with lattice results is even better than for the muon. Also, the estimated model error leads to only  $\sim 5\%$  deviation between full model and error set results.

As full results for the hadronic vacuum polarization contribution to the anomalous magnetic moment of  $\mu$  and  $\tau$  leptons, we report

$$\begin{aligned} a_\mu^{HVP} &= 695.1 \cdot 10^{-10} \\ a_\tau^{HVP} &= 350.2 \cdot 10^{-8}. \end{aligned} \tag{4.45}$$

| $a_\tau^{HVP}$ in $\cdot 10^{-8}$ | $u$   | $d$  | $s$  | $c$  | $b$ (disc.) | $\Sigma$ |
|-----------------------------------|-------|------|------|------|-------------|----------|
| DSE/BSE error                     | 219.8 | 54.9 | 38.1 | 23.7 | 0.7         | 337.3    |
| DSE/BSE base                      | 230.9 | 57.7 | 35.4 | 23.7 | 0.7         | 348.5    |
| DSE/BSE base <sup>QED</sup>       | 230.7 | 57.7 | 35.4 | 23.6 | 0.7         | 348.1    |
| DSE/BSE $\Delta m_q$              | 233.4 | 57.3 | 35.4 | 23.7 | 0.7         | 350.5    |
| DSE/BSE $\Delta m_q^{QED}$        | 233.2 | 57.3 | 35.4 | 23.6 | 0.7         | 350.2    |
| BMWC                              | 281.4 | -    | 36.1 | 22.6 | -2.4        | 341.1    |

Table IV: HVP contributions to the anomalous magnetic moment of the  $\tau$  lepton. As in table III, we compare to lattice data from [84]. The lattice overall result is again only almost the sum of all contributions. Disconnected lattice contributions are still listed in the  $b$  quark column.

## 5 Corrections to couplings and the weak mixing angle

We know that any process in particle physics, if it is observed precisely enough, is subject to hadronic contributions as we analyzed before. Besides the anomalous magnetic moments of leptons, we looked into corrections to  $\alpha_{QED}$  and  $\sin^2(\theta_W)$ , the weak mixing angle, following the lead of [30]. These lattice calculations focus on quark-connected hadronic corrections in leading order in a  $N_f = 2 + 1 + 1$  ensemble. We apply our method to implement hadronic corrections in isospin limit as well as separately for  $u$ - and  $d$ -quark, and compare our findings to referred lattice results and if available to experimental findings collected in [86]. Chapter 5 summarizes this analysis.

### 5.1 Electromagnetic coupling

We start with corrections to the electromagnetic coupling constant  $\alpha_{QED}$ . So far, these corrections have been investigated mostly by lattice [87–89] and dispersive approaches [63,86]. With the tools, we acquired by calculating the anomalous magnetic moment, we are well equipped to take a look ourselves.

The general form of radiative corrections of  $\alpha_{QED}$  is [90]

$$\alpha_{QED}(Q^2) = \frac{\alpha_0}{1 - \Delta\alpha_{QED}(Q^2)},$$

resumming the photon propagator. As usually,  $\alpha_0 \simeq 1/137.036$  at zero momentum transfer  $Q^2 = 0$ . The treatment of the photon propagator is now exactly as in the hadronic corrections to  $a_\mu$ , where all physical information is included in  $\Pi_R(Q^2)$ . Leading order effects on  $\alpha_{QED}$  are identified [86] as

$$\Delta\alpha_{QED}^{HVP}(Q^2) = 4\pi\alpha_0\Pi_R(Q^2),$$

and can immediately be calculated. At this point we stress out again that our polarization function is neither extracted from dispersion relations nor piece wise constructed as most other approaches require. As the whole approach is based on quark-connected contributions, different flavors can be treated separately.

Table I shows results for  $\Delta\alpha_{QED}^{HVP}(Q^2)$  in a momentum range between 0 and 10 GeV<sup>2</sup> from lattice, dispersive analyses and our baseline calculations. Figure 5.1 shows the same results for better overview. It seems that the our result closes in on lattice and dispersive results for higher momenta, but in the lower energy region we clearly overshoot the available data. Contrary to  $a_\mu$ , where we clearly see a influence of at least the quark mass splitting, all results with our different sets produce basically the same results. We show these in Table II.

| $Q^2$ [GeV <sup>2</sup> ] | DSE/BSE | lattice         | disp. relation |
|---------------------------|---------|-----------------|----------------|
| 0.02                      | 0.175   | 0.163(05)(09)   | 0.174(02)      |
| 1                         | 3.899   | 3.721(96)(145)  | 3.651(40)      |
| 2                         | 5.278   | 4.993(102)(144) | 4.916(61)      |
| 3                         | 6.062   | 5.800(111)(151) | 5.725(74)      |
| 4                         | 6.565   | 6.396(108)(156) | 6.333(84)      |
| 6                         | 7.632   | 7.264(114)(159) | 7.223(98)      |
| 8                         | 7.934   | 7.906(124)(151) | 7.850(107)     |
| 10                        | 8.371   | 8.419(130)(159) | 8.420(114)     |

Table I: DSE/BSE corrections to the electromagnetic coupling compared to lattice calculations and dispersive results for baseline quark masses. Dispersive results were taken from [86]. All results are listed in [ $\cdot 10^{-3}$ ].

| $Q^2$ [GeV <sup>2</sup> ] | base, noQED | base, QED | $\Delta m_q$ , noQED | $\Delta m_q$ , QED |
|---------------------------|-------------|-----------|----------------------|--------------------|
| 0.02                      | 0.175       | 0.175     | 0.178                | 0.177              |
| 1                         | 3.899       | 3.895     | 3.926                | 3.922              |
| 2                         | 5.278       | 5.274     | 5.307                | 5.303              |
| 3                         | 6.062       | 6.057     | 6.091                | 6.086              |
| 4                         | 6.565       | 6.561     | 6.595                | 6.590              |
| 6                         | 7.632       | 7.627     | 7.662                | 7.656              |
| 8                         | 7.934       | 7.929     | 7.964                | 7.958              |
| 10                        | 8.371       | 8.366     | 8.401                | 8.396              |

Table II: DSE/BSE corrections to the electromagnetic coupling in various settings. We compare standard masses without QED extension, standard masses with QED model, model masses without QED and the full model. All results are listed in [ $\cdot 10^{-3}$ ].

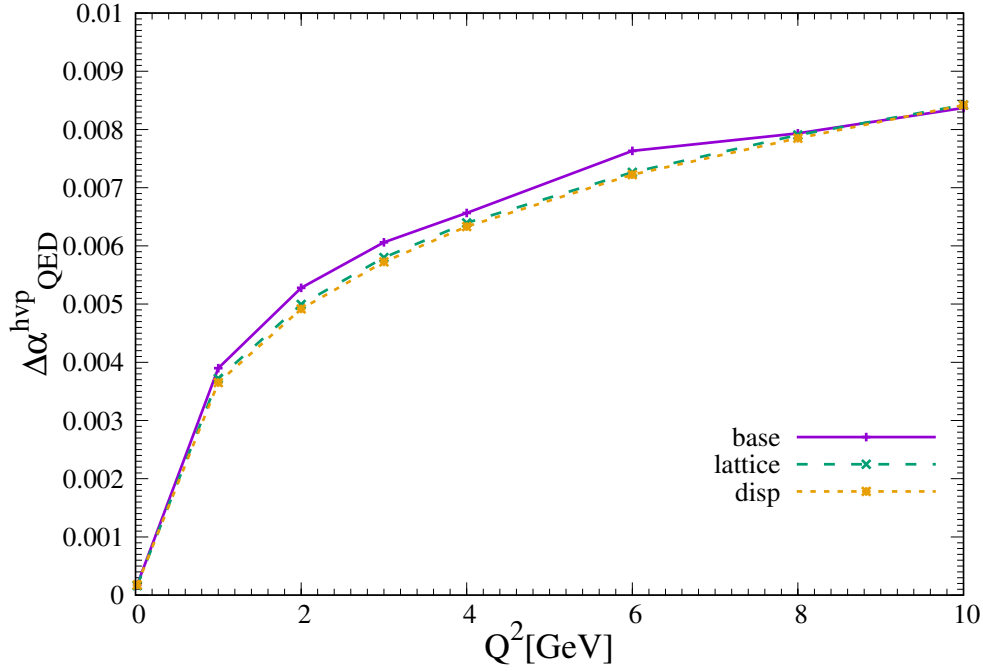


Figure 5.1: Leading order HVP contributions to  $\alpha_{QED}$ . We show a comparison between the data we calculated without any model extensions to the baseline setting, lattice data and results from a dispersive approach.

## 5.2 $SU(2)_L$ coupling and the weak mixing angle

Extracting the leading order hadronic corrections of the coupling  $\alpha_2$  is not as straightforward as the electromagnetic counterpart. Unlike the resummed photon, we have to investigate a mixing between the bosons, namely the  $Z$ - $\gamma$  mixing. To do so, we have to define the relevant currents [86, 90].

$$\begin{aligned}
 J_\mu^\gamma &= \sum_f q^f \bar{\psi}_f \gamma_\mu \psi_f \\
 J_\mu^3 &= \frac{1}{4} \sum_f \bar{\psi}_f \gamma_\mu (1 - \gamma_5) \psi_f \\
 J_\mu^Z &= J_\mu^3 - \sin^2(\theta_W) J_\mu^\gamma
 \end{aligned}$$

The current  $J_\mu^\gamma$  corresponds to the photon,  $J_\mu^3$  to the third component of the weak isospin and  $J_\mu^Z$  as a mix of the two above to the Z-boson, thus the object of interest. In all currents we sum over all quark flavors  $f$ . We already see that in leading order the Z-boson can be treated as if there was no mixing, the problem at hand reduces to a  $\gamma - Z$ -mixing

$$\Pi^{Z\gamma} \simeq \Pi^{3\gamma} = \langle J_\mu^3 J_\nu^\gamma \rangle.$$

Indeed, we can go even further in simplifying by looking at the structure of the two currents  $J_\mu^3$  and  $J_\nu^\gamma$ . We know that photons behave as vector currents. At the same time the third isospin component has a part which behaves as a vector, and an axial-vector part which gets subtracted. Since in our approach vector and axial-vector currents are strictly orthogonal, we don't even have to consider the axial-vector part and end up at

$$\langle J_\mu^3 J_\nu^\gamma \rangle = \langle (V - A)V \rangle = \langle VV \rangle = \Pi_{\mu\nu}^{\gamma\gamma}, \quad (5.1)$$

which is the electromagnetic polarization tensor. This means the leading order correction to the weak coupling  $\alpha_2$ , actually depends on the same function as  $\Delta\alpha_{QED}$ , we only have to take the different charges of the respective interaction into account, the coupling  $g^2$  instead of the electromagnetic charge  $e^2$ .

Connecting all findings above, we are able to look into hadronic corrections to the mixing angle  $\sin^2(\theta_W)$ . This angle, defined by

$$\sin^2(\theta_W) = \frac{e^2}{g^2} = \frac{\alpha_{QED}}{\alpha_2} \quad (5.2)$$

connects electromagnetic and weak interaction via the electroweak unification condition stated above. Thus, having calculated corrections to  $\alpha_{QED}$  and  $\alpha_2$  immediately allows us to extract corrections to  $\sin^2(\theta_W)$ . To do so, we rely on the zero momentum transfer values  $\sin^2(\theta_0)^{ex} = 0.2356(20)$ , and  $\sin^2(\theta_0)^{th} = 0.23871(9)$  which are the experimental [91] and standard model results [92, 93]. In leading order logarithmic approximation we have [94]

$$\sin^2(\theta_W) = \sin^2(\theta_0) \frac{1 - \Delta\alpha_2(Q^2)}{1 - \Delta\alpha_{QED}(Q^2)} = \sin^2(\theta_0) (1 + \Delta(Q^2)) \quad (5.3)$$

with

$$\Delta(Q^2) = \Delta\sin^2(\theta_W) = \Delta\alpha_{QED}(Q^2) - \Delta\alpha_2(Q^2). \quad (5.4)$$

Calculating the final corrections is straight forward and is summarized in table III and plotted in figure 5.2. As with  $\alpha_{QED}$ , the influence of our model corrections are shown in the separate table IV.

The behavior of the results is analogous to the electromagnetic coupling corrections. Our calculations now undershoot the lattice results, and start to close in for higher  $Q^2$ . The corrections to the weak mixing angle, as  $\Delta\alpha_{QED}^{HVP}$  only depend on the hadronic vacuum polarization function, we are not unduly surprised. We actually experienced similar findings in the case of the Adler function in [50]. Again, isospin symmetry breaking effects are not in a numerically relevant range.

| $Q^2$ [GeV <sup>2</sup> ] | DSE/BSE | lattice          |
|---------------------------|---------|------------------|
| 0.02                      | -1.698  | -0.158(05)(08)   |
| 1                         | -3.885  | -3.706(83)(127)  |
| 2                         | -5.285  | -5.021(96)(135)  |
| 3                         | -6.106  | -5.801(104)(135) |
| 4                         | -6.665  | -6.398(102)(135) |
| 6                         | -7.633  | -7.251(111)(136) |
| 8                         | -8.100  | -7.867(112)(137) |
| 10                        | -8.566  | -8.352(119)(138) |

Table III: Corrections to the sine squared of the weak mixing angle. We compare our baseline calculation to lattice data. All results are listed in  $[\cdot 10^{-3}]$ .

| $Q^2$ [GeV <sup>2</sup> ] | base, noQED | base, QED | model, noQED | model QED |
|---------------------------|-------------|-----------|--------------|-----------|
| 0.02                      | -1.698      | -1.696    | -1.704       | -1.702    |
| 1                         | -3.885      | -3.883    | -3.892       | -3.889    |
| 2                         | -5.285      | -5.283    | -5.293       | -5.289    |
| 3                         | -6.106      | -6.103    | -6.113       | -6.110    |
| 4                         | -6.665      | -6.662    | -6.673       | -6.669    |
| 6                         | -7.633      | -7.629    | -7.640       | -7.636    |
| 8                         | -8.100      | -8.096    | -8.107       | -8.103    |
| 10                        | -8.566      | -8.563    | -8.574       | -8.569    |

Table IV: Comparison of the influence of model extension to the weak mixing angle. Since dispersive approaches lack reliable data, a reasonable comparison to experimental values is not possible right now. A list of experiments possibly leading to relevant data is given in [30]. All results are listed in  $[\cdot 10^{-3}]$ .

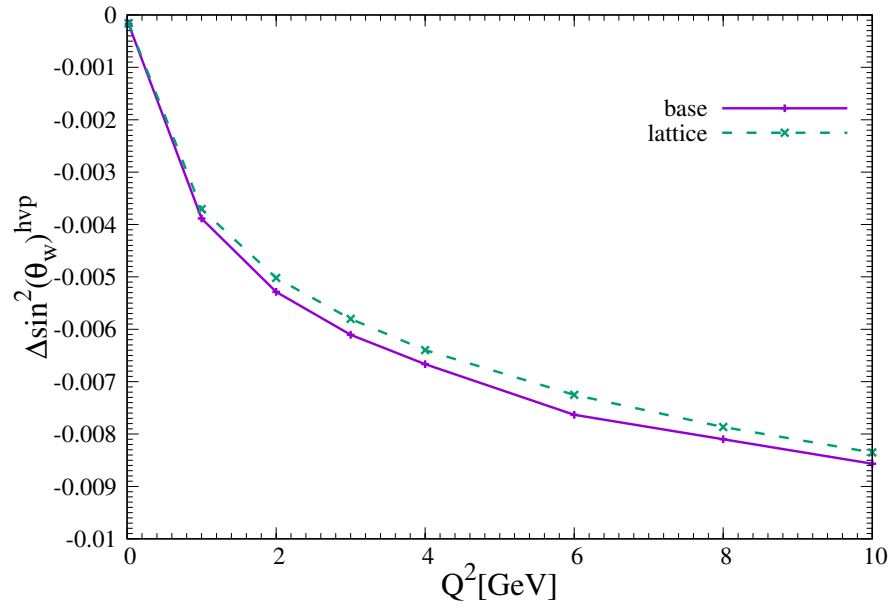


Figure 5.2: Leading order hadronic corrections to the sine squared of the weak mixing angle. We show lattice data and our baseline results.



## 6 Summary

In this chapter, we summarize the motivation and implementation of the isospin symmetry breaking model extension we implemented in quark DSE, bound state meson BSE and the quark-photon vertex. We add some final words about potential further research.

Following a general presentation of the used method, we focused on giving an insight in the motivation behind the modifications we developed. We identified the observed behavior of quarks and bound state masses to find a phenomenological approach to include isospin symmetry breaking effects in our calculations. The different contributions from quark mass splitting and electromagnetic effects were tested against each other and baseline values calculated with a standard RL-MT model.

We were able to confirm that the expected dominance of electromagnetic corrections to the pion mass splitting is upheld in the DSE/BSE framework. Even with a maximum value for a quark current mass splitting of  $\Delta m_q = 6.6$  MeV the observed pion masses varied only by a value of  $M_{\pi^\pm} - M_{\pi^0} = 0.2$  MeV which can be considered to be in a range of numerical uncertainty.

Including QED diagrams in quark and meson calculations on the other hand showed promising behavior. By separately performing calculations with electromagnetic contributions in DSE and/or BSE, we isolated the according influence on the bound state masses. While quark corrections were implemented to always simulate an effectively raised mass, the meson diagrams were used to favor final states with overall neutral charge, by lowering their calculated mass. The used truncation of the quark-photon vertex was influenced by the Ball-Chiu vertex, and models a 1BC-like vertex with additional strengthening factor. This treatment allowed us to find a quark mass set of  $m_u = 2.45$  MeV,  $m_d = 4.61$  MeV and  $m_s = 84.88$  MeV which reproduce physical masses for  $M_{\pi^\pm}$ ,  $M_{\pi^0}$ ,  $M_{K^\pm}$  and  $M_{K^0}$  simultaneously. The quadratic correlation between quark and pion mass is preserved. The almost quark mass independent mass shift between charged and neutral pion mass is effectively a correction exclusively induced by QED inclusion.

The influence of the model in the vector meson channel was found to be minimal. We observe a similar picture to the pion case. Quark mass changes induce a rho

| $a_\mu^{HVP}$ in $\cdot 10^{-10}$ | $u$   | $d$   | $s$  | $c$  | $b$ (disc.) | $\Sigma$ |
|-----------------------------------|-------|-------|------|------|-------------|----------|
| DSE/BSE base                      | 501.3 | 125.3 | 50.4 | 11.0 | 0.0         | 687.7    |
| DSE/BSE $\Delta m_q$              | 510.9 | 123.4 | 50.4 | 10.8 | 0.0         | 695.1    |
| BMWC                              | 674.5 | -     | 53.7 | 14.7 | -12.8       | 711.0    |
| Disp.                             | -     | -     | -    | -    | -           | 694.9    |

Table I: HVP contributions to the anomalous magnetic moment of the  $\mu$  lepton. We show contributions by quark content, and the complete sum. Lattice data was published by the Budapest-Marseille-Wuppertal collaboration [84]. The lattice result does not sum up, since numerous corrections were administered to the final result, which are not listed for separate quark masses. The dispersion relation result was taken from [63].

| $a_\tau^{HVP}$ in $\cdot 10^{-8}$ | $u$   | $d$  | $s$  | $c$  | $b$ (disc.) | $\Sigma$ |
|-----------------------------------|-------|------|------|------|-------------|----------|
| DSE/BSE base                      | 230.9 | 57.7 | 35.4 | 23.7 | 0.7         | 348.5    |
| DSE/BSE model                     | 233.2 | 57.3 | 35.4 | 23.6 | 0.7         | 350.2    |
| BMWC                              | 281.4 | -    | 36.1 | 22.6 | -2.4        | 341.1    |

Table II: HVP contributions to the anomalous magnetic moment of the  $\tau$  lepton.

mass splitting below numerical accuracy. As a difference, the QED extension yields only a mass difference of  $M_{\rho^\pm} - M_{\rho^0} \simeq 0.5$  MeV. While the experimental data does indeed show no rho splitting, we are aware of crucial missing physical precesses as the  $\rho - \omega$  mixing which are not included in the model. We nonetheless see the result as a small step to understanding the rho. Changes in the phi meson are negligible as well, which further supports the understanding that the vector mesons are less dependent on quark masses in general. To define a model error estimate, we set up a quark mass set reproducing physical vector masses. The difference between calculations to results acquired with this mass set was taken as uncertainty.

The main motivation to investigate isospin symmetry breaking was our ongoing research on the anomalous magnetic moment of the muon. Implementing our extended model via modified quark and quark-photon vertex let us analyze changes induced by the different quark masses and QED contributions. We use different model parameters compared to prior results, amounting to a much better overall result for the hadronic vacuum polarization. Though the calculation is essentially the same for the other leptons, the numerical implementation was not stable enough to calculate results for the electron. Results for muon and tau are summarized in tables I and II and compared to lattice and dispersive calculations. As final overall results we give for the hadronic vacuum polarization part of the muon anomalous magnetic moment in the isospin limit and with isospin symmetry breaking model with an estimated

---

model uncertainty of around 10%

$$a_{\mu, isospin \text{ symm.}}^{HVP} = 687.7 \cdot 10^{-10} \quad (6.1)$$

$$a_{\mu, isospin \text{ broken}}^{HVP} = 695.1 \cdot 10^{-10}. \quad (6.2)$$

For the tau lepton, we report

$$a_{\tau, isospin \text{ symm.}}^{HVP} = 348.46 \cdot 10^{-8} \quad (6.3)$$

$$a_{\tau, isospin \text{ broken}}^{HVP} = 350.18 \cdot 10^{-8}. \quad (6.4)$$

An alternative use of the hadronic polarization function is its role in the correction to the electromagnetic coupling  $\alpha_{QED}$  and the weak mixing angle, which was brought to our attention by [30]. The results for both observables agree reasonably well with lattice and experiment, for a first try. While isospin breaking corrections lead to better agreement to dispersive results in the case of magnetic moments, it seems that any change to the isospin symmetric calculation is not reflected in the calculated results.

Work on this topic is not, and probably will not be in near future, concluded yet. Further research beyond the always interesting questions of applicable DSE truncations and their corresponding bound state kernels, are for example different approaches to the constructing of neutral states. A different construction of  $\pi^0$  will have some impact on model parameters in our calculations. Already mentioned was  $\rho - \omega$  mixing, which is in itself an interesting topic. Similar to the truncation question, a more sophisticated investigation on the quark-photon vertex in our model extension might lead to new insights. Last but not least, we might be able to identify and calculate additional observables using explicitly  $\Pi_R$ , as, with enhanced numerical stability the electron anomalous magnetic moment  $a_e$ .



# 7 Appendix

## 7.1 Hyperspherical coordinates

Integration measure in hyperspherical coordinates to make use of symmetries

$$\int \frac{d^4}{(2\pi)^4} \rightarrow \frac{1}{(2\pi)^4} \int d(k^2) \frac{k^2}{2} \int_{-1}^1 dz \sqrt{1-z^2} \int_{-1}^1 dy \int_0^{2\pi} d\phi \quad (7.1)$$

and the parameterization of the integration momentum  $k$

$$k = \sqrt{k^2} \begin{pmatrix} \sqrt{1-z^2} \sqrt{1-y^2} \sin \phi \\ \sqrt{1-z^2} \sqrt{1-y^2} \cos \phi \\ y \sqrt{1-z^2} \\ z \end{pmatrix} \quad (7.2)$$

In BSEs, it is convenient to chose the total momentum  $P$  in the rest-frame. The parameterization can then be simplified as follows

$$P = (0, 0, 0, \sqrt{P^2})^T \quad (7.3)$$

$$p = \sqrt{p^2} (0, 0, \sqrt{1-z_p^2}, z_p)^T \quad (7.4)$$

$$k = \sqrt{k^2} (0, \sqrt{1-z^2} \sqrt{1-y^2}, y \sqrt{1-z^2}, z)^T \quad (7.5)$$



## 8 Bibliography

- [1] M. Gell-Mann, “A schematic model of baryons and mesons,” *Physics Letters* **8** no. 3, (1964) 214 – 215. <http://www.sciencedirect.com/science/article/pii/S0031916364920013>.
- [2] E. D. Bloom, D. H. Coward, H. DeStaebler, J. Drees, G. Miller, L. W. Mo, R. E. Taylor, M. Breidenbach, J. I. Friedman, G. C. Hartmann, and H. W. Kendall, “High-energy inelastic  $e - p$  scattering at  $6^\circ$  and  $10^\circ$ ,” *Phys. Rev. Lett.* **23** (Oct, 1969) 930–934. <https://link.aps.org/doi/10.1103/PhysRevLett.23.930>.
- [3] M. Breidenbach, J. I. Friedman, H. W. Kendall, E. D. Bloom, D. H. Coward, H. DeStaebler, J. Drees, L. W. Mo, and R. E. Taylor, “Observed behavior of highly inelastic electron-proton scattering,” *Phys. Rev. Lett.* **23** (Oct, 1969) 935–939. <https://link.aps.org/doi/10.1103/PhysRevLett.23.935>.
- [4] **Particle Data Group** Collaboration, C. Patrignani *et al.*, “Review of Particle Physics,” *Chin. Phys.* **C40** no. 10, (2016) 100001.
- [5] F. J. Dyson, “The S matrix in quantum electrodynamics,” *Phys. Rev.* **75** (1949) 1736–1755.
- [6] J. S. Schwinger, “On the Green’s functions of quantized fields. 1.,” *Proc. Nat. Acad. Sci.* **37** (1951) 452–455.
- [7] P. Maris, C. D. Roberts, and P. C. Tandy, “Pion mass and decay constant,” *Phys. Lett.* **B420** (1998) 267–273, [arXiv:nuc1-th/9707003](https://arxiv.org/abs/nuc1-th/9707003) [nuc1-th].
- [8] P. Maris and C. D. Roberts, “Pi- and K meson Bethe-Salpeter amplitudes,” *Phys. Rev.* **C56** (1997) 3369–3383, [arXiv:nuc1-th/9708029](https://arxiv.org/abs/nuc1-th/9708029) [nuc1-th].
- [9] P. Maris and P. C. Tandy, “The Quark photon vertex and the pion charge radius,” *Phys.Rev.* **C61** (2000) 045202, [arXiv:nuc1-th/9910033](https://arxiv.org/abs/nuc1-th/9910033) [nuc1-th].
- [10] P. Maris and P. C. Tandy, “Bethe-Salpeter study of vector meson masses and decay constants,” *Phys. Rev.* **C60** (1999) 055214, [arXiv:nuc1-th/9905056](https://arxiv.org/abs/nuc1-th/9905056) [nuc1-th].

- [11] C. S. Fischer and R. Williams, “Beyond the rainbow: Effects from pion back-coupling,” *Phys. Rev. D* **78** (Oct, 2008) 074006.  
<https://link.aps.org/doi/10.1103/PhysRevD.78.074006>.
- [12] M. S. Bhagwat and P. Maris, “Vector meson form factors and their quark-mass dependence,” *Phys. Rev.* **C77** (2008) 025203, [arXiv:nucl-th/0612069](#) [nucl-th].
- [13] H. Sanchis-Alepuz, R. Alkofer, and C. S. Fischer, “Electromagnetic transition form factors of baryons in the space-like momentum region,”  
[arXiv:1707.08463](#) [hep-ph].
- [14] H. Sanchis-Alepuz and R. Williams, “Recent developments in bound-state calculations using the Dyson-Schwinger and Bethe-Salpeter equations,”  
[arXiv:1710.04903](#) [hep-ph].
- [15] H. Sanchis-Alepuz, C. S. Fischer, and S. Kubrak, “Pion cloud effects on baryon masses,” *Phys. Lett.* **B733** (2014) 151–157, [arXiv:1401.3183](#) [hep-ph].
- [16] H. Sanchis-Alepuz and R. Williams, “Hadronic Observables from Dyson-Schwinger and Bethe-Salpeter equations,” *J. Phys. Conf. Ser.* **631** no. 1, (2015) 012064, [arXiv:1503.05896](#) [hep-ph].
- [17] G. Eichmann, C. S. Fischer, and W. Heupel, “Four-point functions and the permutation group  $S_4$ ,” *Phys. Rev.* **D92** no. 5, (2015) 056006,  
[arXiv:1505.06336](#) [hep-ph].
- [18] G. Eichmann, C. S. Fischer, and W. Heupel, “Tetraquarks from the Bethe-Salpeter equation,” *Acta Phys. Polon. Supp.* **8** (2015) 425,  
[arXiv:1507.05022](#) [hep-ph].
- [19] G. Eichmann, C. S. Fischer, and W. Heupel, “The light scalar mesons as tetraquarks,” *Phys. Lett.* **B753** (2016) 282–287, [arXiv:1508.07178](#) [hep-ph].
- [20] W. Heupel, *Light tetraquarks and mesons in a DSE/BSE approach*. PhD thesis, Giessen U., 2015. [http://geb.uni-giessen.de/geb/volltexte/2015/11607/pdf/HeupelWalter\\_2015\\_07\\_09.pdf](http://geb.uni-giessen.de/geb/volltexte/2015/11607/pdf/HeupelWalter_2015_07_09.pdf).
- [21] H. Sanchis-Alepuz and C. S. Fischer, “Hyperon elastic electromagnetic form factors in the space-like momentum region,” *Eur. Phys. J.* **A52** no. 2, (2016) 34, [arXiv:1512.00833](#) [hep-ph].
- [22] G. Eichmann, H. Sanchis-Alepuz, R. Williams, R. Alkofer, and C. S. Fischer, “Baryons as relativistic three-quark bound states,” *Prog. Part. Nucl. Phys.* **91** (2016) 1–100, [arXiv:1606.09602](#) [hep-ph].



- 
- [23] E. Weil, G. Eichmann, C. S. Fischer, and R. Williams, “Electromagnetic decays of the neutral pion,” *Phys. Rev.* **D96** no. 1, (2017) 014021, [arXiv:1704.06046 \[hep-ph\]](#).
  - [24] G. Eichmann, C. Fischer, E. Weil, and R. Williams, “On the large- $Q^2$  behavior of the pion transition form factor,” *Phys. Lett.* **B774** (2017) 425–429, [arXiv:1704.05774 \[hep-ph\]](#).
  - [25] C. S. Fischer, T. Goecke, and R. Williams, “A fresh look at hadronic light-by-light scattering in the muon  $g-2$  with the Dyson-Schwinger approach,” *Eur.Phys.J.* **A47** (2011) 28, [arXiv:1009.5297 \[hep-ph\]](#).
  - [26] T. Goecke, C. S. Fischer, and R. Williams, “Hadronic light-by-light scattering in the muon  $g-2$ : a Dyson-Schwinger equation approach,” *Phys.Rev.* **D83** (2011) 094006, [arXiv:1012.3886 \[hep-ph\]](#).
  - [27] T. Goecke, C. S. Fischer, and R. Williams, “Leading-order calculation of hadronic contributions to the muon  $g - 2$  using the Dyson-Schwinger approach,” *Phys.Lett.* **B704** (2011) 211–217, [arXiv:1107.2588 \[hep-ph\]](#).
  - [28] T. Goecke, C. S. Fischer, and R. Williams, “The role of momentum dependent dressing functions and vector meson dominance in hadronic light-by-light contributions to the muon  $g - 2$ ,” *Phys.Rev.* **D87** no. 3, (2013) 034013, [arXiv:1210.1759 \[hep-ph\]](#).
  - [29] G. Eichmann, C. S. Fischer, W. Heupel, and R. Williams, “The muon  $g-2$ : Dyson-Schwinger status on hadronic light-by-light scattering,” *AIP Conf. Proc.* **1701** (2016) 040004, [arXiv:1411.7876 \[hep-ph\]](#).
  - [30] F. Burger, K. Jansen, M. Petschlies, and G. Pientka, “Leading hadronic contributions to the running of the electroweak coupling constants from lattice qcd,” *Journal of High Energy Physics* **2015** no. 11, (Nov, 2015) 215. [https://doi.org/10.1007/JHEP11\(2015\)215](https://doi.org/10.1007/JHEP11(2015)215).
  - [31] C. Becchi, A. Rouet, and R. Stora, “The Abelian Higgs-Kibble Model. Unitarity of the S Operator,” *Phys. Lett.* **52B** (1974) 344–346.
  - [32] J. C. Taylor, “Ward Identities and Charge Renormalization of the Yang-Mills Field,” *Nucl. Phys.* **B33** (1971) 436–444.
  - [33] A. A. Slavnov, “Ward identities in gauge theories,” *Theoretical and Mathematical Physics* **10** no. 2, (Feb, 1972) 99–104. <https://doi.org/10.1007/BF01090719>.
  - [34] C. S. Fischer, “Infrared properties of QCD from Dyson-Schwinger equations,” *J. Phys.* **G32** (2006) R253–R291, [arXiv:hep-ph/0605173](#).

- [35] R. Alkofer and L. von Smekal, “The infrared behavior of QCD Green’s functions: Confinement, dynamical symmetry breaking, and hadrons as relativistic bound states,” *Phys. Rept.* **353** (2001) 281, [arXiv:hep-ph/0007355](#).
- [36] S. L. Adler, “Axial vector vertex in spinor electrodynamics,” *Phys. Rev.* **177** (1969) 2426–2438.
- [37] J. M. Cornwall, R. Jackiw, and E. Tomboulis, “Effective Action for Composite Operators,” *Phys. Rev.* **D10** (1974) 2428–2445.
- [38] H. Munczek, “Dynamical chiral symmetry breaking, Goldstone’s theorem and the consistency of the Schwinger-Dyson and Bethe-Salpeter Equations,” *Phys.Rev.* **D52** (1995) 4736–4740, [arXiv:hep-th/9411239](#) [hep-th].
- [39] A. Krassnigg, “Survey of J=0,1 mesons in a Bethe-Salpeter approach,” *Phys. Rev.* **D80** (2009) 114010, [arXiv:0909.4016](#) [hep-ph].
- [40] W. Heupel, T. Goecke, and C. S. Fischer, “Beyond Rainbow-Ladder in bound state equations,” *Eur. Phys. J.* **A50** (2014) 85, [arXiv:1402.5042](#) [hep-ph].
- [41] H. Sanchis-Alepuz, S. D. Kubrak, and C. S. Fischer, “Beyond Rainbow-Ladder in a covariant three-body Bethe-Salpeter approach: Baryons,” *EPJ Web Conf.* **73** (2014) 04019, [arXiv:1402.1013](#) [hep-ph].
- [42] R. Williams, C. S. Fischer, and W. Heupel, “Light mesons in QCD and unquenching effects from the 3PI effective action,” *Phys. Rev.* **D93** no. 3, (2016) 034026, [arXiv:1512.00455](#) [hep-ph].
- [43] A. Krassnigg, “Excited mesons in a Bethe-Salpeter approach,” *PoS CONFINEMENT8* (2008) 075, [arXiv:0812.3073](#) [nucl-th].
- [44] N. I. Ioakimidis, K. E. Papadakis, and E. A. Perdios, “Numerical evaluation of analytic functions by cauchy’s theorem,” *BIT Numerical Mathematics* **31** no. 2, (Jun, 1991) 276–285. <https://doi.org/10.1007/BF01931287>.
- [45] J.-P. Berrut and L. N. Trefethen, “Barycentric lagrange interpolation,” *SIAM Review* **46** no. 3, (2004) 501–517, <https://doi.org/10.1137/S0036144502417715>, <https://doi.org/10.1137/S0036144502417715>.
- [46] C. S. Fischer, D. Nickel, and R. Williams, “On Gribov’s supercriticality picture of quark confinement,” *Eur. Phys. J.* **C60** (2009) 47–61, [arXiv:0807.3486](#) [hep-ph].

- 
- [47] E. E. Salpeter and H. A. Bethe, “A Relativistic equation for bound state problems,” *Phys. Rev.* **84** (1951) 1232–1242.
- [48] N. Nakanishi, “Normalization Condition and Normal and Abnormal Solutions of the Bethe-Salpeter Equation,” *Phys. Rev.* **138** (1965) B1182–B1192.
- [49] C.-S. Huang, H.-Y. Jin, and Y.-B. Dai, “Bethe-salpeter wave functions for mesons of arbitrary spin and the covariant instantaneous approximation,” *Phys. Rev. D* **51** (Mar, 1995) 2347–2352.  
<https://link.aps.org/doi/10.1103/PhysRevD.51.2347>.
- [50] T. Göckel, *Hadronic Contributions to the anomalous Magnetic Moment of the Muon*. PhD thesis, Universität Gießen, 2012.
- [51] M. Gell-Mann, R. J. Oakes, and B. Renner, “Behavior of current divergences under  $SU(3) \times SU(3)$ ,” *Phys. Rev.* **175** (1968) 2195–2199.
- [52] W. Bietenholz *et al.*, “Flavour blindness and patterns of flavour symmetry breaking in lattice simulations of up, down and strange quarks,” *Phys. Rev. D* **84** (2011) 054509, [arXiv:1102.5300](https://arxiv.org/abs/1102.5300) [hep-lat].
- [53] R. Horsley *et al.*, “QED effects in the pseudoscalar meson sector,” *JHEP* **04** (2016) 093, [arXiv:1509.00799](https://arxiv.org/abs/1509.00799) [hep-lat].
- [54] J. S. Ball and T.-W. Chiu, “Analytic Properties of the Vertex Function in Gauge Theories. 1.,” *Phys. Rev. D* **22** (1980) 2542.
- [55] C. S. Fischer, P. Watson, and W. Cassing, “Probing unquenching effects in the gluon polarisation in light mesons,” *Phys. Rev. D* **72** (2005) 094025, [arXiv:hep-ph/0509213](https://arxiv.org/abs/hep-ph/0509213) [hep-ph].
- [56] W. N. Cottingham, “The neutron proton mass difference and electron scattering experiments,” *Annals Phys.* **25** (1963) 424–432.
- [57] W. A. Bardeen, J. Bijnens, and J.-M. Gérard, “Hadronic matrix elements and the  $\pi^+-\pi^0$  mass difference,” *Phys. Rev. Lett.* **62** (Mar, 1989) 1343–1346.  
<https://link.aps.org/doi/10.1103/PhysRevLett.62.1343>.
- [58] S. Aoki *et al.*, “Review of lattice results concerning low-energy particle physics,” *Eur. Phys. J. C* **74** (2014) 2890, [arXiv:1310.8555](https://arxiv.org/abs/1310.8555) [hep-lat].
- [59] H. B. O’Connell, B. C. Pearce, A. W. Thomas, and A. G. Williams, “ $\rho - \omega$  mixing, vector meson dominance and the pion form-factor,” *Prog. Part. Nucl. Phys.* **39** (1997) 201–252, [arXiv:hep-ph/9501251](https://arxiv.org/abs/hep-ph/9501251) [hep-ph].

- [60] D. Hanneke, S. Fogwell, and G. Gabrielse, “New Measurement of the Electron Magnetic Moment and the Fine Structure Constant,” *Phys. Rev. Lett.* **100** (2008) 120801, [arXiv:0801.1134 \[physics.atom-ph\]](#).
- [61] **E34** Collaboration, M. Otani, “Status of the Muon g-2/EDM Experiment at J-PARC (E34),” *JPS Conf. Proc.* **8** (2015) 025008.
- [62] B. Roberts, “Status of the Fermilab Muon (g-2) Experiment,” *Chin. Phys.* **C34** (2010) 741–744, [arXiv:1001.2898 \[hep-ex\]](#).
- [63] F. Jegerlehner and A. Nyffeler, “The Muon g-2,” *Phys. Rept.* **477** (2009) 1–110, [arXiv:0902.3360 \[hep-ph\]](#).
- [64] F. J. M. Farley and Y. K. Semertzidis, “The 47 years of muon g-2,” *Prog. Part. Nucl. Phys.* **52** (2004) 1–83.
- [65] S. Goudschmidt and G. Uhlenbeck, “Spinning electrons and the structure of spectra,” *Nature* **117** (1926) 264–265.
- [66] P. A. Dirac, “The Quantum theory of electron,” *Proc. Roy. Soc. Lond.* **A117** (1928) 610–624.
- [67] P. Kusch and H. M. Foley, “Precision measurement of the ratio of the atomic ‘g values’ in the  $^2p_{3/2}$  and  $^2p_{1/2}$  states of gallium,” *Phys. Rev.* **72** (Dec, 1947) 1256–1257. <http://link.aps.org/doi/10.1103/PhysRev.72.1256.2>.
- [68] J. Schwinger, “On quantum-electrodynamics and the magnetic moment of the electron,” *Phys. Rev.* **73** (Feb, 1948) 416–417. <http://link.aps.org/doi/10.1103/PhysRev.73.416>.
- [69] M. E. Peskin and D. V. Schroeder, *An Introduction To Quantum Field Theory (Frontiers in Physics)*. Westview Press, 1995.
- [70] J. Aldins, T. Kinoshita, S. J. Brodsky, and A. Dufner, “Photon - photon scattering contribution to the sixth order magnetic moments of the muon and electron,” *Phys. Rev.* **D1** (1970) 2378.
- [71] R. Barbieri and E. Remiddi, “Electron and Muon 1/2(g-2) from Vacuum Polarization Insertions,” *Nucl. Phys.* **B90** (1975) 233–266.
- [72] T. Aoyama, M. Hayakawa, T. Kinoshita, and M. Nio, “Complete Tenth-Order QED Contribution to the Muon g-2,” [arXiv:1205.5370 \[hep-ph\]](#).
- [73] A. Czarnecki, W. J. Marciano, and A. Vainshtein, “Refinements in electroweak contributions to the muon anomalous magnetic moment,” *Phys. Rev.* **D67** (2003) 073006, [arXiv:hep-ph/0212229 \[hep-ph\]](#).

- 
- [74] K. Hagiwara, R. Liao, A. D. Martin, D. Nomura, and T. Teubner, “ $(g - 2)_\mu$  and  $\alpha(M_Z^2)$  re-evaluated using new precise data,” *J. Phys.* **G38** (2011) 085003, [arXiv:1105.3149 \[hep-ph\]](#).
  - [75] S. Eidelman, F. Jegerlehner, A. L. Kataev, and O. Veretin, “Testing nonperturbative strong interaction effects via the Adler function,” *Phys. Lett.* **B454** (1999) 369–380, [arXiv:hep-ph/9812521 \[hep-ph\]](#).
  - [76] J. Prades, E. de Rafael, and A. Vainshtein, “Hadronic Light-by-Light Scattering Contribution to the Muon Anomalous Magnetic Moment,” [arXiv:0901.0306 \[hep-ph\]](#).
  - [77] T. Lee and C.-N. Yang, “Question of Parity Conservation in Weak Interactions,” *Phys.Rev.* **104** (1956) 254–258.
  - [78] J. Bailey, W. Bartl, G. von Bochmann, R. C. A. Brown, F. J. M. Farley, M. Giesch, H. Jostlein, S. van der Meer, E. Picasso, and R. W. Williams, “Precise Measurement of the Anomalous Magnetic Moment of the Muon,” *Nuovo Cim.* **A9** (1972) 369–432.
  - [79] **CERN Muon Storage Ring** Collaboration, J. Bailey *et al.*, “The Anomalous Magnetic Moment of Positive and Negative Muons,” *Phys. Lett.* **67B** (1977) 225. [*Phys. Lett.*68B,191(1977)].
  - [80] **Muon G-2 Collaboration** Collaboration, G. Bennett *et al.*, “Final Report of the Muon E821 Anomalous Magnetic Moment Measurement at BNL,” *Phys.Rev.* **D73** (2006) 072003, [arXiv:hep-ex/0602035 \[hep-ex\]](#).
  - [81] E. de Rafael, “Hadronic contributions to the muon g-2 and low-energy QCD,” *Phys.Lett.* **B322** (1994) 239–246, [arXiv:hep-ph/9311316 \[hep-ph\]](#).
  - [82] R. Alkofer, C. S. Fischer, F. J. Llanes-Estrada, and K. Schwenzer, “The Quark-gluon vertex in Landau gauge QCD: Its role in dynamical chiral symmetry breaking and quark confinement,” *Annals Phys.* **324** (2009) 106–172, [arXiv:0804.3042 \[hep-ph\]](#).
  - [83] N. Brown and M. R. Pennington, “Studies of Confinement: How the Gluon Propagates,” *Phys. Rev.* **D39** (1989) 2723.
  - [84] **Budapest-Marseille-Wuppertal** Collaboration, S. Borsanyi *et al.*, “Hadronic vacuum polarization contribution to the anomalous magnetic moments of leptons from first principles,” [arXiv:1711.04980 \[hep-lat\]](#).
  - [85] **Fermilab Lattice, LATTICE-HPQCD, MILC** Collaboration, B. Chakraborty *et al.*, “Strong-isospin-breaking correction to the muon

- anomalous magnetic moment from lattice QCD at the physical point,” [arXiv:1710.11212 \[hep-lat\]](#).
- [86] F. Jegerlehner, “Electroweak effective couplings for future precision experiments,” *Nuovo Cim.* **C034S1** (2011) 31–40, [arXiv:1107.4683 \[hep-ph\]](#).
- [87] D. B. Renner, X. Feng, K. Jansen, and M. Petschlies, “Nonperturbative QCD corrections to electroweak observables,” *PoS LATTICE2011* (2012) 022, [arXiv:1206.3113 \[hep-lat\]](#).
- [88] X. Feng, G. Hotzel, K. Jansen, M. Petschlies, and D. B. Renner, “Leading-order hadronic contributions to  $a_\mu$  and  $\alpha_{QED}$  from  $N_f = 2 + 1 + 1$  twisted mass fermions,” *PoS LATTICE2012* (2012) 174, [arXiv:1211.0828 \[hep-lat\]](#).
- [89] **European Twisted Mass** Collaboration, R. Baron *et al.*, “Computing K and D meson masses with  $N_f = 2+1+1$  twisted mass lattice QCD,” *Comput. Phys. Commun.* **182** (2011) 299–316, [arXiv:1005.2042 \[hep-lat\]](#).
- [90] F. Jegerlehner, “Hadronic Contributions to Electroweak Parameter Shifts: A Detailed Analysis,” *Z. Phys.* **C32** (1986) 195.
- [91] V. A. Dzuba, J. C. Berengut, V. V. Flambaum, and B. Roberts, “Revisiting parity non-conservation in cesium,” *Phys. Rev. Lett.* **109** (2012) 203003, [arXiv:1207.5864 \[hep-ph\]](#).
- [92] J. Erler and M. J. Ramsey-Musolf, “The Weak mixing angle at low energies,” *Phys. Rev.* **D72** (2005) 073003, [arXiv:hep-ph/0409169 \[hep-ph\]](#).
- [93] K. S. Kumar, S. Mantry, W. J. Marciano, and P. A. Souder, “Low Energy Measurements of the Weak Mixing Angle,” *Ann. Rev. Nucl. Part. Sci.* **63** (2013) 237–267, [arXiv:1302.6263 \[hep-ex\]](#).
- [94] F. Jegerlehner, “Vector Boson Parameters: Scheme Dependence and Theoretical Uncertainties,” *Z. Phys.* **C32** (1986) 425. [Erratum: *Z. Phys.* **C38**, 519 (1988)].

## Erklärung

Ich erkläre: Ich habe die vorgelegte Dissertation selbstständig und ohne unerlaubte fremde Hilfe und nur mit den Hilfen angefertigt, die ich in der Dissertation angegeben habe. Alle Textstellen, die wörtlich oder sinngemäß aus veröffentlichten Schriften entnommen sind, und alle Angaben, die auf mündlichen Auskünften beruhen, sind als solche kenntlich gemacht. Ich stimme einer evtl. Überprüfung meiner Dissertation durch eine Antiplagiat-Software zu. Bei den von mir durchgeführten und in der Dissertation erwähnten Untersuchungen habe ich die Grundsätze guter wissenschaftlicher Praxis, wie sie in der “Satzung der Justus-Liebig-Universität Gießen zur Sicherung guter wissenschaftlicher Praxis” niedergelegt sind, eingehalten.

Gießen, June 14, 2018

---

Jan Bonnet